

Supporting Information

An optimized polyamine moiety boosts potency of human type II topoisomerase poisons as quantified by comparative analysis centered on the clinical candidate F14512

Giulia Palermo,¹ Elirosa Minniti,¹ Maria Laura Greco,² Laura Riccardi,¹ Elena Simoni,³ Marino Convertino,¹ Chiara Marchetti,³ Michela Rosini,³ Claudia Sissi,² Anna Minarini³ and Marco De Vivo^{1*}

1. Laboratory of Molecular Modeling and Drug Discovery, Istituto Italiano di Tecnologia, Via Morego 30, 16163 Genoa, Italy;

2. Department of Pharmaceutical and Pharmacological Sciences, University of Padova, Via Marzolo 5, 35131 Padova, Italy;

3. Department of Pharmacy and Biotechnology, Alma Mater Studiorum-University of Bologna, Via Belmeloro 6, 40126 Bologna, Italy

Supporting:

Page S2-S17: Computational methods and additional figures

Page S18: Molecular biology

Page S19- S40: Medicinal Chemistry

Supplementary Text

Computational Material and Methods

Structural Models. MD simulations have been based on the crystallographic structure of the human topoisomerase II β (topoll) in complex with DNA and etoposide (i.e., ternary complex), solved at 2.16 Å resolution (pdb code 3QX3).¹ The protein is an homodimer, composed by Monomer A and Monomer B. Few missing residues of the protein, which are far from the cleavage complex, were modeled using PRIME, based on the x-ray structure of the topoll/DNA binary complex, solved at 2.98 Å resolution (3L4K).² Two simulations systems of the topoll/DNA cleavage complex bound to etoposide and the F14512 have been built, namely ETOcc and F14cc. The initial binding pose of etoposide has been taken from the crystallographic coordinates recently published by Wu et al.¹ The initial pose of F14512 has been generated via automated docking procedure using the software Glide.³⁻⁵ During the docking procedure, a positional restraint has been applied on the epipodophyllotoxin moiety of F14512 to reproduce the binding of the same core characterizing the drug etoposide.¹ All the amine groups of F14512 have been considered as protonated at physiological pH (7.4). Protonation states have been predicted at a target pKa of 10^{-7.4}, using the Epik software for predicting pKa values for drug-like molecules.⁶

Molecular Dynamics (MD) Simulations. Molecular dynamics (MD) was used to equilibrate the complexes (ETOcc and F14cc) at physiological conditions and for the production runs. The AMBER force field ff99SB27 with the ff99Bldn38 modifications was adopted for the protein, whereas the parmbsc049 modification of the AMBER parm99 force field was adopted for the DNA. We used the Åqvist510 force field parameters for the Mg²⁺ ions, as in our previous study of the Topoll catalytic mechanism.¹¹ The etoposide and F14512 molecules were treated with the General Amber Force Field (GAFF),¹² and the atomic charges were derived by the RESP fitting procedure.¹³ The systems were immersed in a box of TIP3P¹⁴ water molecules (producing a total of ~220.000 atoms for each of the two systems) of edge 130x140x140 Å³, in a ~10 mM buffer of MgCl₂. This large simulation box has been necessary in order to allow the complete solvation of the drugs outside the binding pocket during the subsequent Steered Molecular Dynamics (SMD) simulations (full details are reported below). A time step set of 2 fs was used. Hydrogen atoms were added assuming standard bond lengths and were constrained to their equilibrium position with the RATTLE¹⁵ algorithm implemented in NAMD 2.8.¹⁶ The systems were studied in the isothermal–isobaric (NPT) ensemble coupled to a Langevin thermostat at 298 K and barostat at 1 atm. Periodic boundary conditions were applied to the systems. PME method was used to evaluate long-range electrostatic interactions, and a cutoff of 12 Å was used to account for the van der Waals interactions. MD simulations were first carried out on the ETOcc system, with the following protocol. First, the system was subjected to energy minimization by using the Steepest Descent algorithm. Then, the system was thermalized up to physiological temperature in the canonical ensemble (NVT) using a Langevin bath in three consecutive steps: (1) the solvent was first equilibrated in ~10 ps of MD, slowly increasing the temperature from 0 to 100 K and maintaining both the protein and the nucleic acid fixed, (2) the temperature was further increased up to 200 K in ~10 ps of MD, while keeping fixed only the coordinates of backbone atoms of the protein/DNA complex, (3) constraints were released and the systems were simulated for ~25 ps of MD to reach the temperature of 298 K. Then,

we switched to the NPT statistical ensemble, performing ~100 ps of MD at 298 K. This approach has been shown to be efficient for the equilibration phase of large biological systems (~200,000 total atoms).¹⁷ After this initial phase, finite temperature MD simulations were performed. After ~200 ns of MD, the Root Mean Square Deviation (RMSD) of the protein and DNA heavy atoms reached a plateau, ensuring the structural stability of the system (Figure S1). The same procedure was applied to the F14cc. Production runs were carried out on both simulation systems in the NPT statistical ensemble. All the MD simulations were performed using the NAMD 2.8.¹⁶ MD code. We obtained ~400 ns of MD at 298 K for the ETOcc system and ~320 ns of MD for the F14cc system, resulting in a total of ~700-800 ns of dynamics. Coordinates of the systems were collected every 2 ps, for a total of ~180/200,000 frames for each system. Due to the reproducibility of the results in both topoll monomers (Figure S2), statistics were collected for both the enzyme subunits of each equilibrated system.

Details on the probability distribution plots in Figure 1C. Figure 1C of the main text reports the time evolution (last 200 ns) of the RMSD for the heavy atoms of the aglycone core (upper graphs), the E-ring (central graphs) and the glycoside/spermine (lower graphs) groups of etoposide (orange) and F14512 (black) in the ETOcc and F14cc systems, for one subunit of topoll (Monomer A). For each set of data, probability distribution plots are reported. A Kernel Density Estimation (KDE) analysis has been performed. KDE functions were used to estimate the probability density function of the RMSD values along the dynamics. KDE is a non-parametric way to estimate the probability density function of a random variable. A kernel is a smooth function centered at the location of each data point. The contributions from each function are summed and plotted. Mathematically, the kernel estimate $f(x)$ for a data set of N points x_i is:

$$[1] \quad f(x) = (1/N) \sum_i^N (1/h) K((x-x_i)/h)$$

where $K(x)$ is any smooth, normalized function, and h is the bandwidth: a measure of the width of the kernel function.

Docking of the etoposide derivatives (F14512 and compounds 3–7). F14512 (**2**) and compounds **3–7** have been docked within the topoll active site using the Glide³⁻⁵ software of the Schrodinger suite.¹⁸ The topoll/DNA cleavage complex (pdb code: 3QX3¹) was prepared with ProteinWizard.¹⁸ The grid for the docking of compounds **2**(F14512)–**7** was centered at the position of etoposide in monomer A, while the maximum size of the docked ligands was set to 36 Å. Positional restraints were set on A-ring and D-ring of the conserved 4'-demethylepipodophyllotoxin core to generate an etoposide-like binding mode.¹ For each ligand, we considered a maximum of 100 poses. The superimposition of all the docking poses of F14512 (**2**) and of compounds **3–7** is reported in Figure S5.

Steered Molecular Dynamics (SMD). We used SMD simulations in order to compare the energetics of binding of etoposide (**1**) and F14512 (**2**) at the topoll/DNA level. Indeed, the ligand-receptor binding/unbinding event is rarely sampled during unbiased nanosecond time-scale MD. In SMD simulations, a time-dependent external force is applied to the ligand to facilitate its unbinding from the protein. The transition between the bound and unbound states is obtained by adding to the standard Hamiltonian a harmonic time-dependent potential $U(r,t)$ acting on a descriptor $s(r)$, namely a pulling variable that can be for instance the distance

between protein and ligand center of masses (COM). During the transition, we can calculate the exerted force and the external work performed on the system, which are a measure of the binding/unbinding propensity. Indeed, since the ligand is harmonically restrained to a constant-velocity moving point, it is possible to obtain the mechanical irreversible work necessary for the undocking by integrating the force exerted on the system along the unbinding reaction coordinate (i.e., the pulling variable). In detail, the applied harmonic time-dependent potential $U(r,t)$ acting on a descriptor $s(r)$, holds the following time-dependency [eq. 1]:

$$[2] \quad U(\mathbf{r}, t) = \frac{k}{2} [s(\mathbf{r}) - s_0(t) - vt]^2$$

where s_0 is the value of the descriptor in the initial state, t is the time, and k is a constant representing the strength of the applied force. After a predetermined amount of time, the harmonic constraint will be centered in its final position [eq. 3]:

$$[3] \quad s_1 = s_0 + vt_1$$

Therefore, at constant pulling velocity, if the spring constant k is large enough (stiff-spring regime), it is reasonable to assume that, at the final time t_1 , the system has approximately reached the point s_1 . During this transition, the value of the exerted force $F(t)$ is calculated using [eq. 4]:

$$[4] \quad F(t) = -k[s(\mathbf{r}) - s_\lambda(t) - vt]$$

while the external work ΔW performed on the system is calculated by integrating the power along the entire transition time [eq. 5]:

$$[5] \quad \Delta W = v \int_{t_0}^{t_1} F(t) dt$$

All the SMD simulations were performed using the PLUMED¹⁹ plugin integrated in the NAMD 2.8 MD code.¹⁶ Since we were interested in the unbinding of the drugs from the protein, we have chosen as a pulling variable the distance between the COM of the aglycone core (drugs) and the COM of one stable part of the protein (i.e., residues 740–752 and 760–772, Figure S8A). Given the structural similarity of monomer A and B, SMD simulations have been performed on one subunit of the topoll/DNA cleavage complex. The choice of stable part of the protein core was done in order to avoid artificial distortions of this latter during SMD as a consequence of the pulling. The pulling parameters were determined by performing different trial simulations in different conditions and by comparing the calculated work values. The final choice has been based on a compromise between accuracy and speed, which is a classical tradeoff in drug design. A spring constant of 1000 kcal/(mol·Å²) along with a pulling velocity of 0.03 Å/ps were chosen. This pulling velocity was shown not to irreversibly disrupt the protein secondary structure (Figure S8B). The target distance for the SMD simulations was

chosen to be 65 Å, which ensured the complete solvation of the drugs outside the binding pocket. The time length for each simulation was ~3 ns, which was sufficient to observe the entire ligand unbinding process. In order to achieve a proper amount of statistics for the derivation of the exerted force [$F(t)$] and the external work [ΔW] performed on the system, we performed multiple SMD simulations starting from different configurations of the ETOcc and F14cc systems. In detail, 50 structural snapshots for each of the ETOcc and F14cc systems have been randomly extracted from our unbiased MD simulation and subjected to 100 independent SMD simulations of ~3 ns length, each. Thus, the conditions for these 100 SMD simulations were different only for the starting configurations and initial velocities. In Figure 3 of the main text, we report the average force profiles as a function of the simulation time obtained from 50 SMD simulations for etoposide (orange) and F14512 (black). At the beginning of each simulation ($t = 0$ ns), the ligand is in the bound state. In detail, when at $t = 0$ ns (i.e., corresponding to unbiased MD simulations), etoposide mainly contacts the protein residues, while F14512 also establishes key interactions with the DNA. After ~0.6 ns, the ligand detaches from their active site, protruding toward the solvent. After ~1.6 ns, the ligand is fully solvated. For both compounds, the force profiles (Figure S9-A) show one peak, which corresponds to the detachment of the ligand from the active site. These peaks correspond to the transient H-bond interactions established by each compound on its exit from the binding site. In particular, we observe a higher force profile for F14512, with respect to etoposide. Indeed, the polyamine chain of F14512 is mainly responsible for the establishment and subsequent disruption of transient H-bonds with the topoll/DNA cleavage complex. Around 2.4 ns, the force profiles are approaching zero, indicating that the ligands are completely dissociated from the topoll/DNA complex. We also report the work necessary for the undocking (Figure S9-B), showing that F14512 needs additional ~80 kcal/mol with respect etoposide.^{20,21} Overall, SMD results corroborate the hypothesis of a critical role of the F14512 polyamine chain at the target level (see the main text).

Supplementary Movie S1. Classical Molecular Dynamic (MD) simulations of the ETOcc system. The protein framework (gray) and the DNA (purple) are shown as ribbons. Etoposide (yellow) and the key protein residues Asp479 and Gln778 (gray) are shown as sticks. The topoll catalytic Mg²⁺ ion is also shown as orange sphere.

Supplementary Movie S2. Classical Molecular Dynamic (MD) simulations of the F14cc system. For sake of clarity, the same representation of the ETOcc system has been adopted.

Supplementary Movie S3. Steered MD (SMD) simulations of the F14cc system. One representative trajectory among 50 SMD simulations of the F14cc system is shown. The protein (gray) is shown in molecular surface, as well as the DNA (purple), which is further highlighted as ribbons and sticks. F14512 (yellow) is shown in space filling representation.

Supplementary Figures and Tables

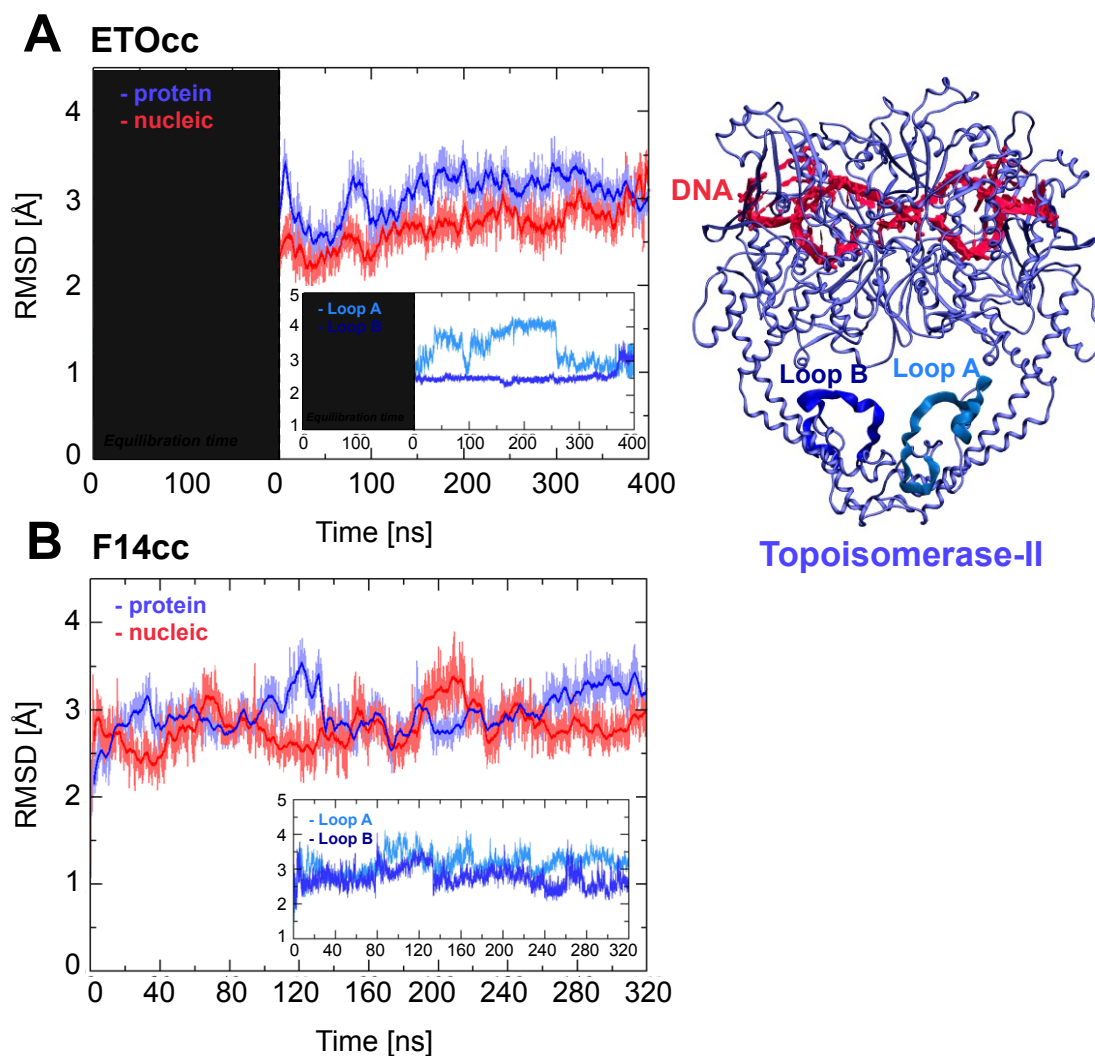


Figure S1. Time evolution of the Root Mean Square Deviation (RMSD) with respect to the initial MD configuration of the protein (blue) and nucleic (red) heavy atoms of the ETOcc (upper panel) and F14cc (lower panel) systems. For the ETOcc system, the time-evolution of the RMSD during the equilibration time (~200 ns) is also shown. The RMSD for the modeled residues – i.e., Loop A (light blue) and Loop B (deep blue) – is shown as an insert in the graphs. The main contribution to the protein RMSD is referred to the larger deviations that are detected for the modeled Loop A and Loop B, both far from the cleavage complex. The RMSD is expressed in Å. The structure of the simulated topolI/DNA cleavage complex stabilized by the anticancer drug etoposide is shown at the top right. The protein (blue) and DNA (red) are shown as ribbons, while Loop A and Loop B are highlighted in light and deep blue, respectively.

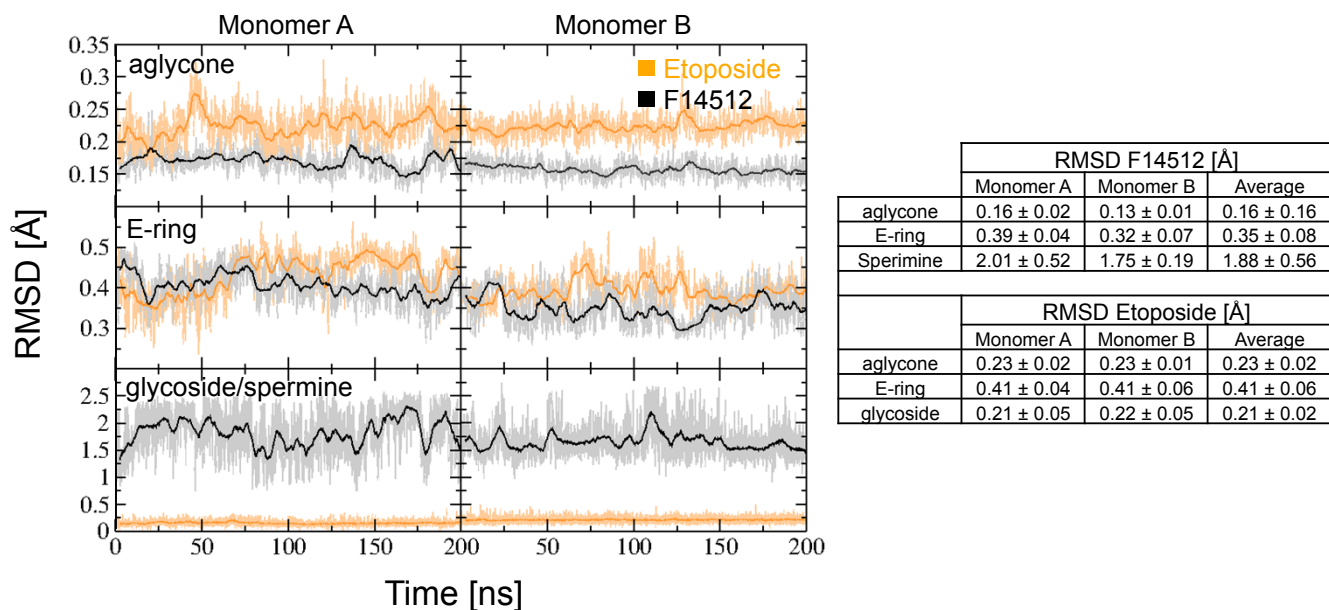
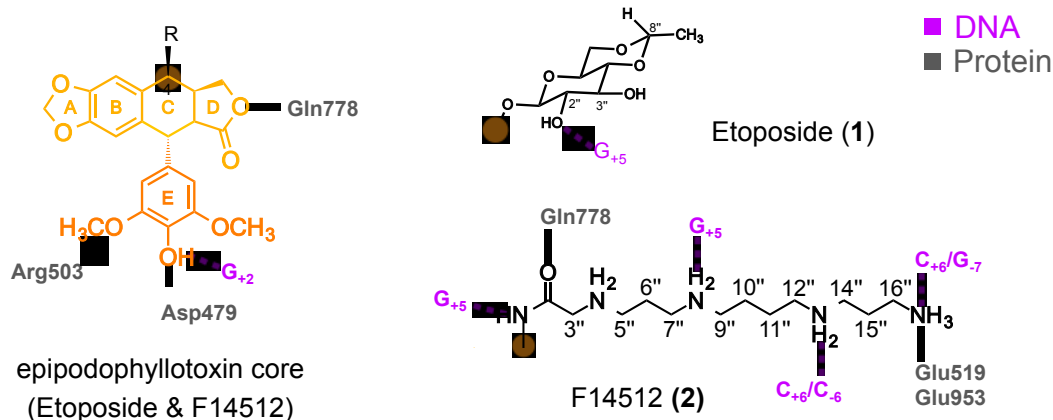


Figure S2. Time evolution along the last ~200 ns of MD simulations of the Root Mean Square Deviation (RMSD) with respect to the initial MD configuration for the heavy atoms of the aglycone core (upper graphs), the E-ring (central graphs) and the glycoside/spermine (lower graphs) groups of etoposide (orange) and F14512 (black) in the ETOcc and F14cc systems. Data are reported for both topoll subunits in the first (Monomer A) and second (Monomer B) columns. The RMSD is expressed in Å. The table on the right reports the average RMSD values along the last ~50 ns of MD.



H-bond occupancy [%]

	H-bond	Etoposide (1)			F14512 (2)		
		Mnr-A	Mnr-B	average	Mnr-A	Mnr-B	average
E-ring	OH-G ₊₂	5.6	4.8	5.2	6.3	5.2	5.8
	OH-Asp479	86.8	78.3	82.6	81.7	74.6	78.7
	H ₃ CO-Arg503	18.2	16.8	17.5	17.9	19.1	18.5
Aglicone	O ₁₂ -Gln778	7.9	6.4	7.2	8.7	5.9	7.3
Spermine (F14512)	O _{2'} -Gln778				8.8	10.2	9.5
	N _{4''} -Gln778				5.3	6.8	6.1
	N _{1''} -O _{base} @G ₊₅				95.5	97.6	96.6
	N _{4''} -O _{hb} @G ₊₅				17.9	10.8	14.4
	N _{8''} -O _{hb} @G ₊₅				39.9	21.4	30.7
	N _{13''} -O _{hb} @G ₊₅				6.6	7.4	7.0
	N _{13''} -O _{hb} @G ₊₆				45.4	38.2	41.8
	N _{13''} -O _{hb} @G ₋₆				52.1	49.7	50.9
	N _{17''} -O _{hb} @G ₊₆				41.2	34.3	37.8
	N _{17''} -O _{hb} @G ₋₆				57.2	54.6	55.9
	N _{17''} -Glu519				8.4	10.2	9.3
N _{17''} -Glu953				14.9	15.7	15.3	
Glycoside (Etoposide)	OH _{2'} -O _{base} @G ₊₅	70.2	72.6	71.4			

Figure S3. Recurrent H-bond interactions between the topolII/DNA cleavage complex and the anticancer drugs etoposide (1) and F14512 (2) are schematically shown on top. The interactions with the protein and DNA components of the cleavage complex are shown in gray and purple, respectively. The table reports the statistical distribution of the H-bonds established by etoposide, F14512 and the topolII/DNA cleavage complex over the last ~200 ns of MD. The statistical distribution of the H-bonds is expressed as H-bond occupancy (i.e., % of simulations time that the H-bond is formed), which has been calculated considering a donor-acceptor distance and angles cutoffs of 3.2 Å and 180 ± 20°, respectively. For sake of clarity, the H-bonds involving the E-ring core, the aglycone and the spermine/glycosidic moieties are highlighted in orange, yellow and black, respectively.

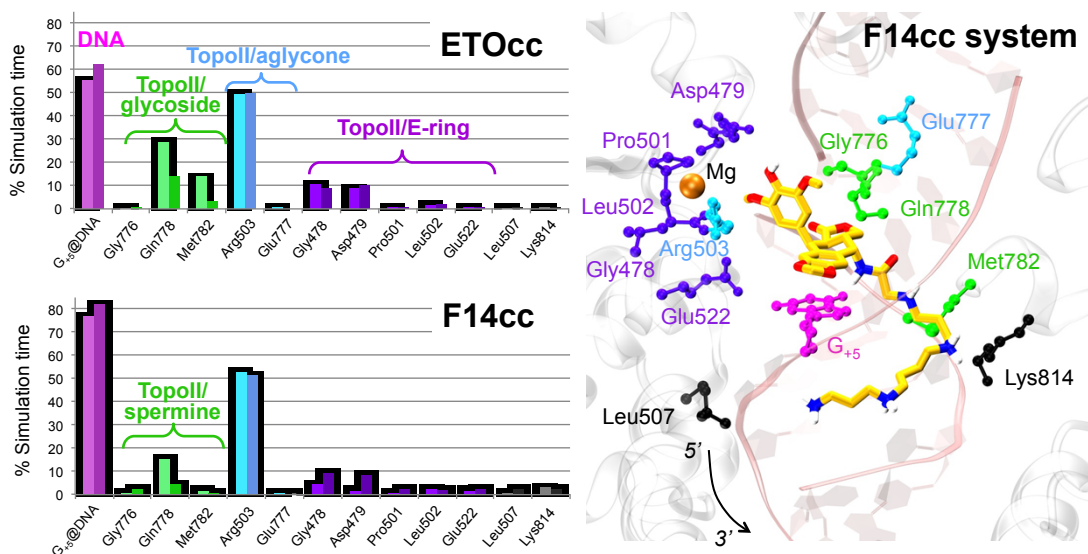


Figure S4. Statistical distribution (% of the total simulation time), over the last ~200 ns of MD simulations, of the direct hydrophobic interactions between the protein residues of the topoll/DNA cleavage complex and the anticancer drugs etoposide (ETOcc system, upper panel) and F14512 (F14cc system, lower panel). Interactions involving topoll residues and the aglycone core, the E-ring and the glycoside/spermine moieties are shown in blue, violet and green bars, respectively. Additional protein-spermine interactions with Lys814 and Leu507 are also reported using black bars. Interactions involving the DNA base G₊₅ and the drugs are shown with magenta bars. Data are reported for both topoll subunits (i.e., Monomer A and B in two adjacent bars). Hydrophobic contacts were counted when nonpolar atoms were separated by at most 4.0 Å. In the right panel, a representative snapshot from MD simulations of the F14cc system is also reported. F14512 (yellow) is shown in sticks. Crucial protein residues interacting with the drugs aglycone core (blue), the E-ring (violet) and the glycoside/spermine moieties (green) are shown in space filling representation. Lys814 and Leu507 (black) are also shown. The protein (gray) and the DNA (purple) are shown in ribbons.

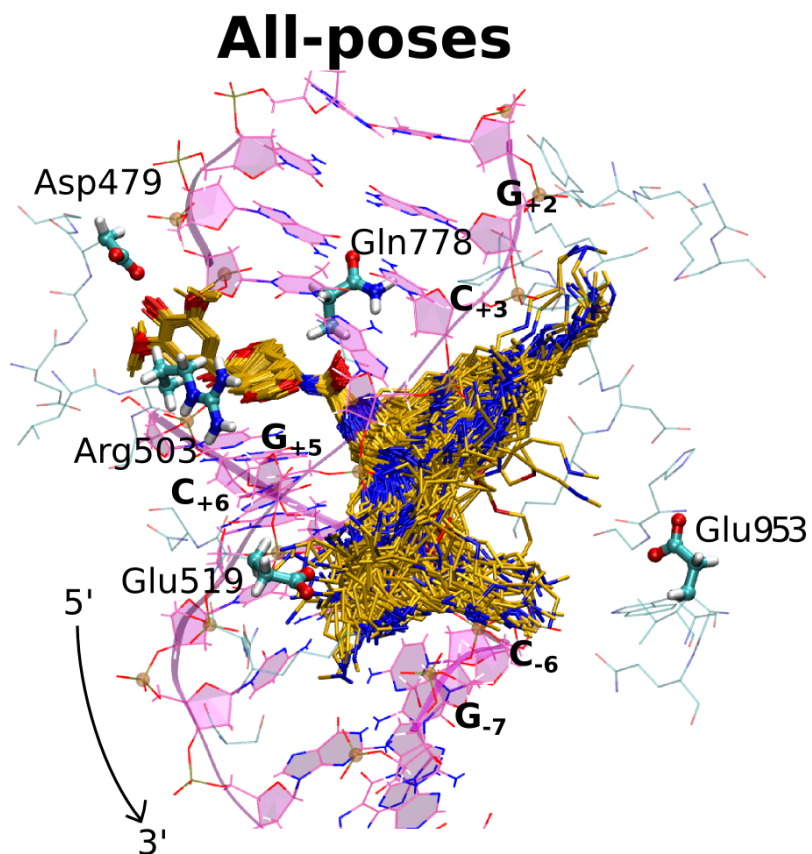


Figure S5. Superposition of all the docking poses of F14512 (**2**) and of compounds **3–7**. The 4'-demethylepipodophyllotoxin core is constrained in the same position as etoposide, with E-ring protruding toward the minor groove, while the long polyamine chains bind in the major groove of the DNA, in a fan-like pattern. The two residues Glu519 and Glu953, which interact with the spermine moiety of F14512 during our MD simulations (see the main text), are also shown.

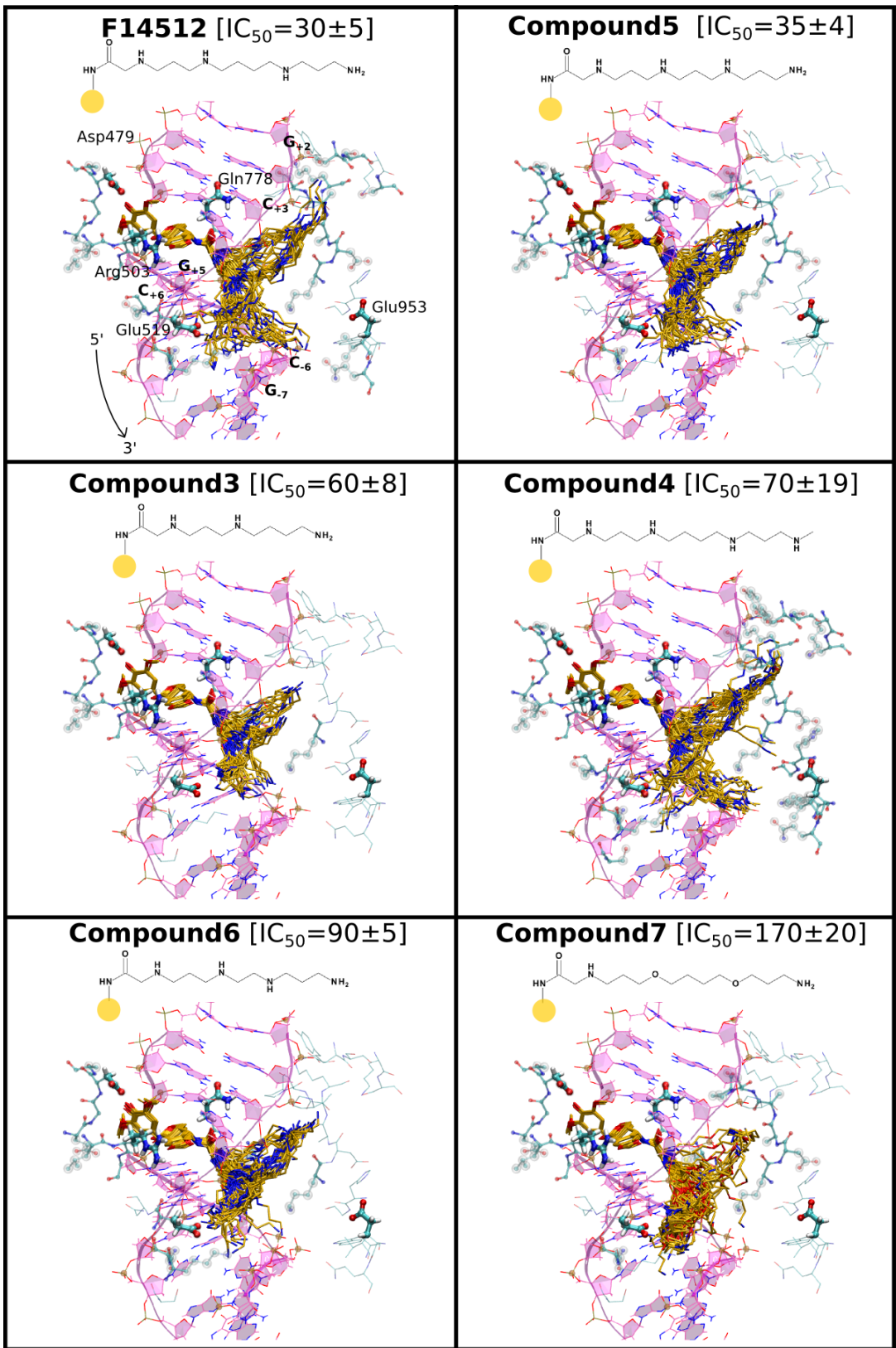


Figure S6. Docking solutions of F14512 (**2**) and compounds **3–7** to the topII/DNA cleavage complex. F14512 and compound **5** have a similar pattern of docking poses, where the polyamine chain points “up” toward C₊₃, or “down” toward C₊₆/Glu519. Interestingly, it can also reach the complementary DNA strand at positions C₋₆/G₋₇, in the direction of Glu953. In MD simulations of the F14cc system, thanks to a rearrangement of the protein structure, Glu593 interacts with N17” of F14512, thus stabilizing this binding mode of the drug into the topII/DNA cleavage complex. Compound **3** has a shorter polyamine chain than that of F14512, which however maintains its nitrogen atoms in position 4”, 8” and 13”. Therefore, the pattern of the docking poses of **3** is similar to that of F14512, as the main DNA contacts are conserved. Compound **6** mainly loses the interactions with the DNA strand of C₋₆/G₋₇. The spacer between the inner N atoms (N8” and N10”) is shorter than in all the other compounds. N10” reaches less efficiently the DNA backbone, thus decreasing the DNA/compound interactions. In **7**, the central amine nitrogen atoms of F14512 are substituted by O8” and O13”. These modifications cause the decrease of the interactions with the DNA. Although **7** maintains the same number of atoms in its chain as F14512, it assumes more curved conformations.

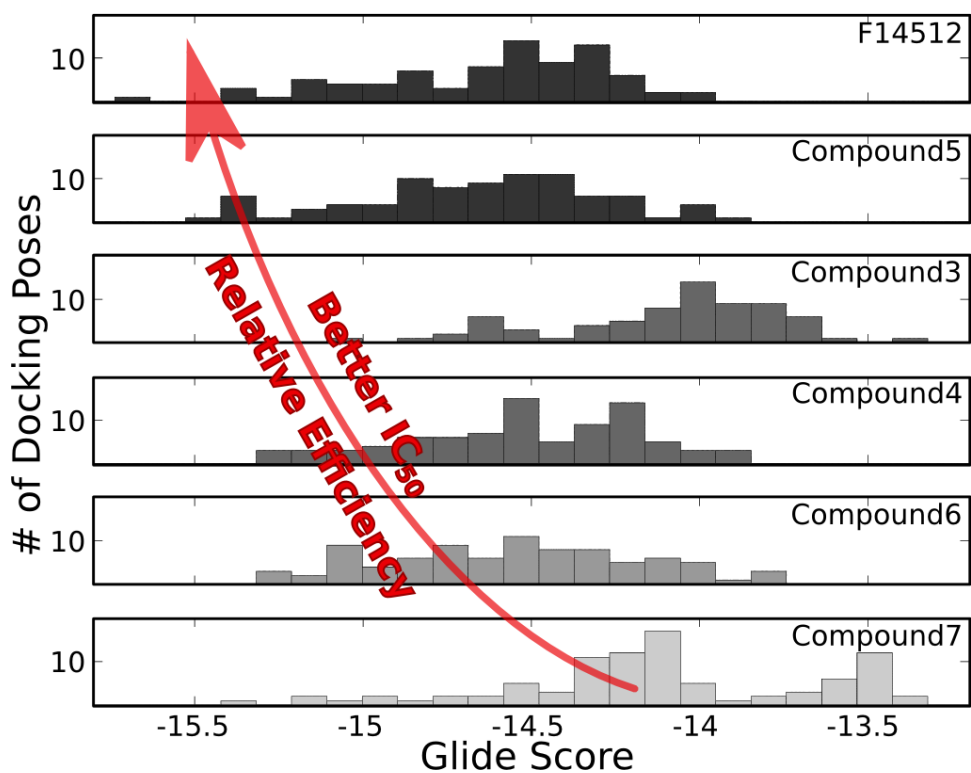


Figure S7. Histogram of the docking scores of F14512 (**2**) and of compounds **3-7**, considering all the poses generated (top ~100 poses). Although only qualitative, the plot shows that the experimental IC₅₀ value and the relative efficiency correlate fairly well with the distribution of Glide Score of the best docking poses. Indeed, moving from Compound **7** to F14512, there is a shift of the distribution of the docking scores toward higher absolute values.

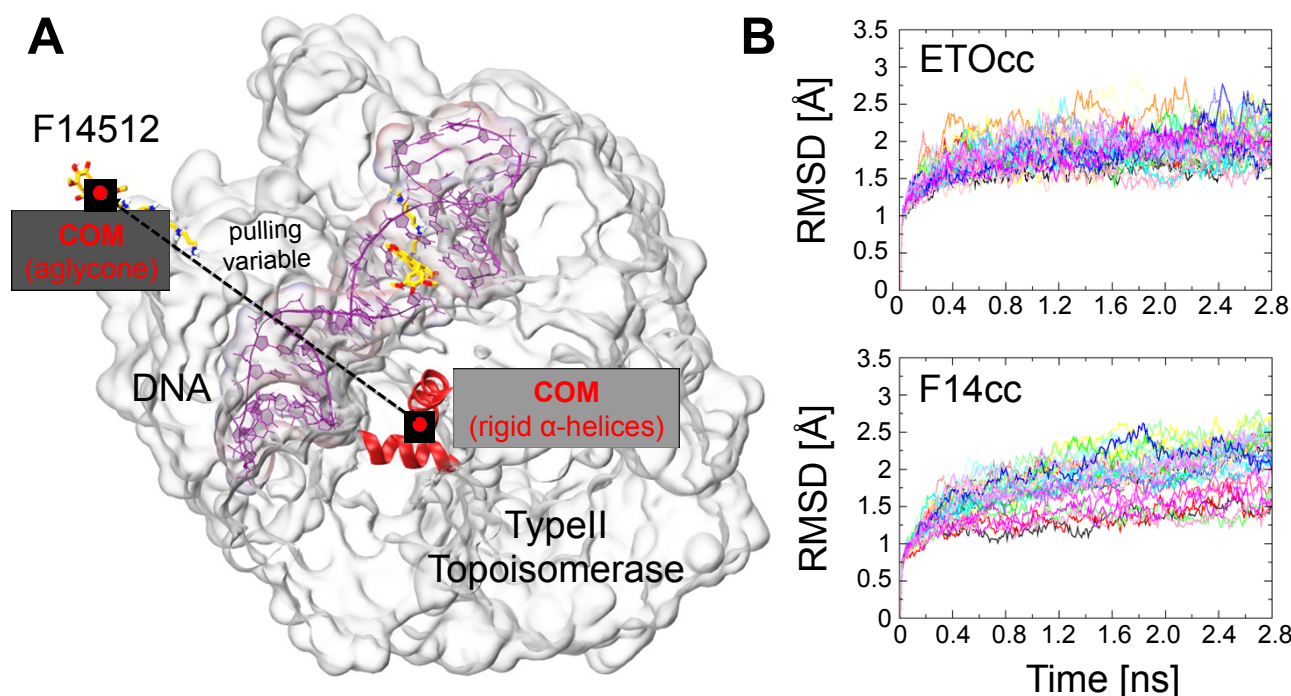


Figure S8. (A) Snapshot from Steered Molecular Dynamics (SMD) of the F14cc system, showing the pulling variable employed in the simulations (see supplementary text for full details). The pulling variable has been defined as the distance between the center of mass (COM) of the aglycone moiety of the drugs and the COM of residues 740–752 and 760–772, which constitute two rigid α -helices of the protein. Topoll (gray) is shown as molecular surface, while the DNA (purple) is represented in ribbons. F14512 (yellow) is shown as sticks. The 740–752 and 760–772 residues of the protein are highlighted using red cartoon. (B) Time evolution of the protein RMSD (heavy atoms) along 50 independent SMD of the ETOcc (upper panel) and F14cc (lower panel) systems. After ~ 0.4 ns, RMSD values reach a plateau at $\sim 2/2.5$ Å, indicating the stability of the protein framework during SMD simulations. This data indicates that the chosen pulling velocity (i.e., 0.03 Å/ps) does not lead to the disruption of the protein secondary structure during SMD simulations.

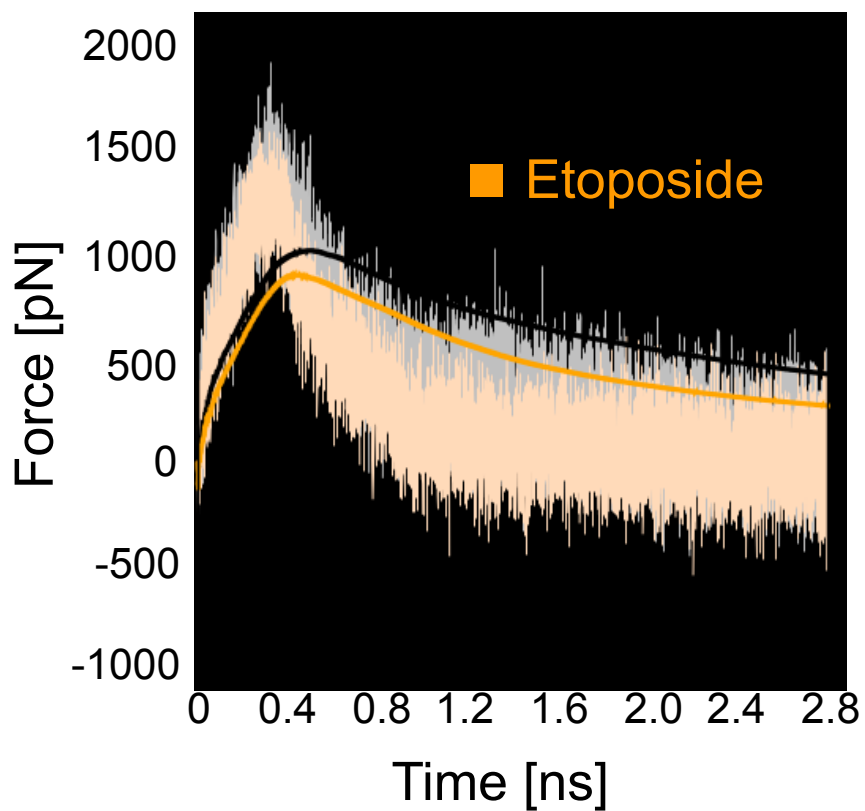


Figure S9. Average force profiles for the undocking of Etoposide (orange) and F14512 (black), as averaged over 50 STM runs for each system, as reported in figure 3. The thick lines highlight the averaged trend of the forces (reported and discussed also in the manuscript, Figure 3).

Compound4

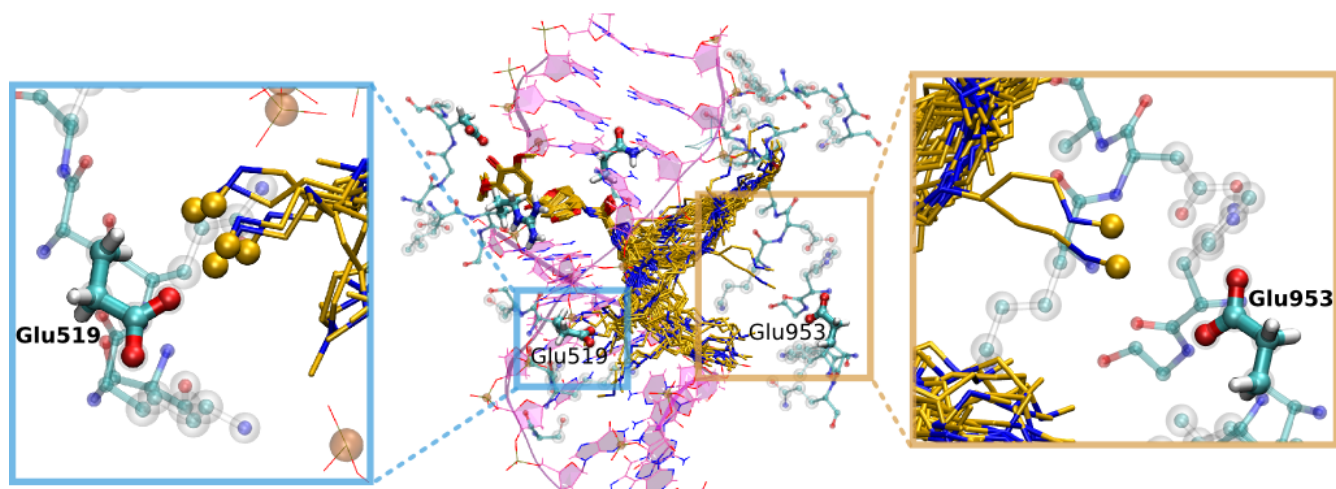
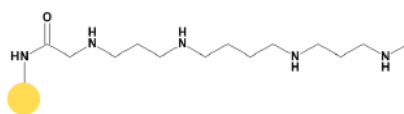


Figure S10. Docking of Compound 4 into the topII/DNA cleavage complex. Compound 4 differs from F14512 for the presence of a secondary amine at position N17". The methyl group of Compound 4 (shown as a gold sphere) lies between N17" and the oxygens of either Glu519 or Glu953. Albeit Compound 4 has a similar length as F14512, the steric hindrance of its methyl group interferes with the formation of an H-bond with topII.

References

- (1) Wu, C. C.; Li, T. K.; Farh, L.; Lin, L. Y.; Lin, T. S.; Yu, Y. J.; Yen, T. J.; Chiang, C. W.; Chan, N. L. *Science* **2011**, *333*, 459.
- (2) Schmidt, B. H.; Burgin, A. B.; Deweese, J. E.; Osheroff, N.; Berger, J. M. *Nature* **2010**, *465*, 641.
- (3) Friesner, R. A.; Banks, J. L.; Murphy, R. B.; Halgren, T. A.; Klicic, J. J.; Mainz, D. T.; Repasky, M. P.; Knoll, E. H.; Shelley, M.; Perry, J. K.; Shaw, D. E.; Francis, P.; Shenkin, P. S. *J Med Chem* **2004**, *47*, 1739.
- (4) Friesner, R. A.; Murphy, R. B.; Repasky, M. P.; Frye, L. L.; Greenwood, J. R.; Halgren, T. A.; Sanschagrin, P. C.; Mainz, D. T. *J Med Chem* **2006**, *49*, 6177.
- (5) Halgren, T. A.; Murphy, R. B.; Friesner, R. A.; Beard, H. S.; Frye, L. L.; Pollard, W. T.; Banks, J. L. *J Med Chem* **2004**, *47*, 1750.
- (6) Shelley, J. C.; Greenwood, J. R.; Timlin, M.; Uchiyama, M.; Shelley, M. *Abstr Pap Am Chem S* **2006**, *232*, 287.
- (7) Hornak, V.; Abel, R.; Okur, A.; Strockbine, B.; Roitberg, A.; Simmerling, C. *Proteins* **2006**, *65*, 712.
- (8) Lindorff-Larsen, K.; Piana, S.; Palmo, K.; Maragakis, P.; Klepeis, J. L.; Dror, R. O.; Shaw, D. E. *Proteins* **2010**, *78*, 1950.
- (9) Perez, A.; Marchan, I.; Svozil, D.; Sponer, J.; Cheatham, T. E., 3rd; Laughton, C. A.; Orozco, M. *Biophysical journal* **2007**, *92*, 3817.
- (10) Aqvist, J. *Journal of Physical Chemistry* **1990**, *94*, 8021.
- (11) Palermo, G.; Stenta, M.; Cavalli, A.; Dal Peraro, M.; De Vivo, M. *J Chem Theory Comput* **2013**, *9*, 857.
- (12) Wang, J.; Wolf, R. M.; Caldwell, J. W.; Kollman, P. A.; Case, D. A. *J Comput Chem* **2004**, *25*, 1157.
- (13) Bayly, C. I.; Cieplak, P.; Cornell, W. D.; Kollman, P. A. *J Phys Chem* **1993** *97*, 10269.
- (14) Jorgensen, W. L.; Chandrasekhar, J.; Madura, J. D.; Impey, R. W.; Klein, M. L. *J Chem Phys* **1983**, *79*, 926
- (15) Andersen, H. C. *J Comput Phys* **1983**, *52*, 24.
- (16) Phillips, J. C.; Braun, R.; Wang, W.; Gumbart, J.; Tajkhorshid, E.; Villa, E.; Chipot, C.; Skeel, R. D.; Kale, L.; Schulten, K. *J Comput Chem* **2005**, *26*, 1781.
- (17) Palermo, G.; Campomanes, P.; Neri, M.; Piomelli, D.; Cavalli, A.; Rothlisberger, U.; De Vivo, M. *J Chem Theory Comput* **2013**, *9*, 1202.
- (18) Sastry, G. M.; Adzhigirey, M.; Day, T.; Annabhimoju, R.; Sherman, W. *J Comput Aid Mol Des* **2013**, *27*, 221.
- (19) Bonomi, M.; Branduardi, D.; Bussi, G.; Camilloni, C.; Provasi, D.; Raiteri, P.; Donadio, D.; Marinelli, F.; Pietrucci, F.; Broglia, R. A.; Parrinello, M. *Computer Physics Communications* **2009**, *180*, 1961.
- (20) Colizzi, F.; Perozzo, R.; Scapozza, L.; Recanatini, M.; Cavalli, A. *Journal of the American Chemical Society* **2010**, *132*, 7361.
- (21) Patel, J. S.; Berteotti, A.; Ronsisvalle, S.; Rocchia, W.; Cavalli, A. *J Chem Inf Model* **2014**, *54*, 470.

Molecular Biology

Topoisomerase inhibition. 0.125 µg of pBR322 (*Inspiralis*) were incubated with increasing concentrations (0.5-200 µM) of tested compounds for 1 hour at 37 °C in the presence/absence of 1 U of human topoisomerase II α (*Inspiralis*) in the required buffer (1X). Reaction products were resolved on a 1% agarose gel prepared in 1X TAE (10mM Tris 1mM EDTA, 0.1% acetic acid, pH 8.0). After the electrophoretic run (5 V/cm for about 90 min) the DNA bands were visualized by ethidium bromide staining, photographed and quantified using a Geliance 2000 apparatus.

Topoisomerase poisoning. 0.125 µg of pBR322 (*Inspiralis*) were incubated with increasing concentrations (0.5-200 µM) of tested compounds for 6 minutes at 37 °C in the presence/absence of 5 U of Topoisomerase II α . Then, the reaction was stopped with 0.1% SDS (Sodium Dodecyl Sulphate, *Sigma*), and finally the enzyme was digested with 1,6µg of proteinase K (*Sigma*) in 10mM Na-EDTA for 30 min at 45 °C. Reaction products were resolved on a 1% agarose gel in 1X TAE (10mM Tris 1mM EDTA, 0.1% acetic acid pH 8.0). The electrophoretic run was performed at 5 V/cm for 90 minutes and then bands were stained with ethidium bromide (0.5 µg/mL in 1X TAE) photographed and quantified using a Geliance 2000 apparatus.

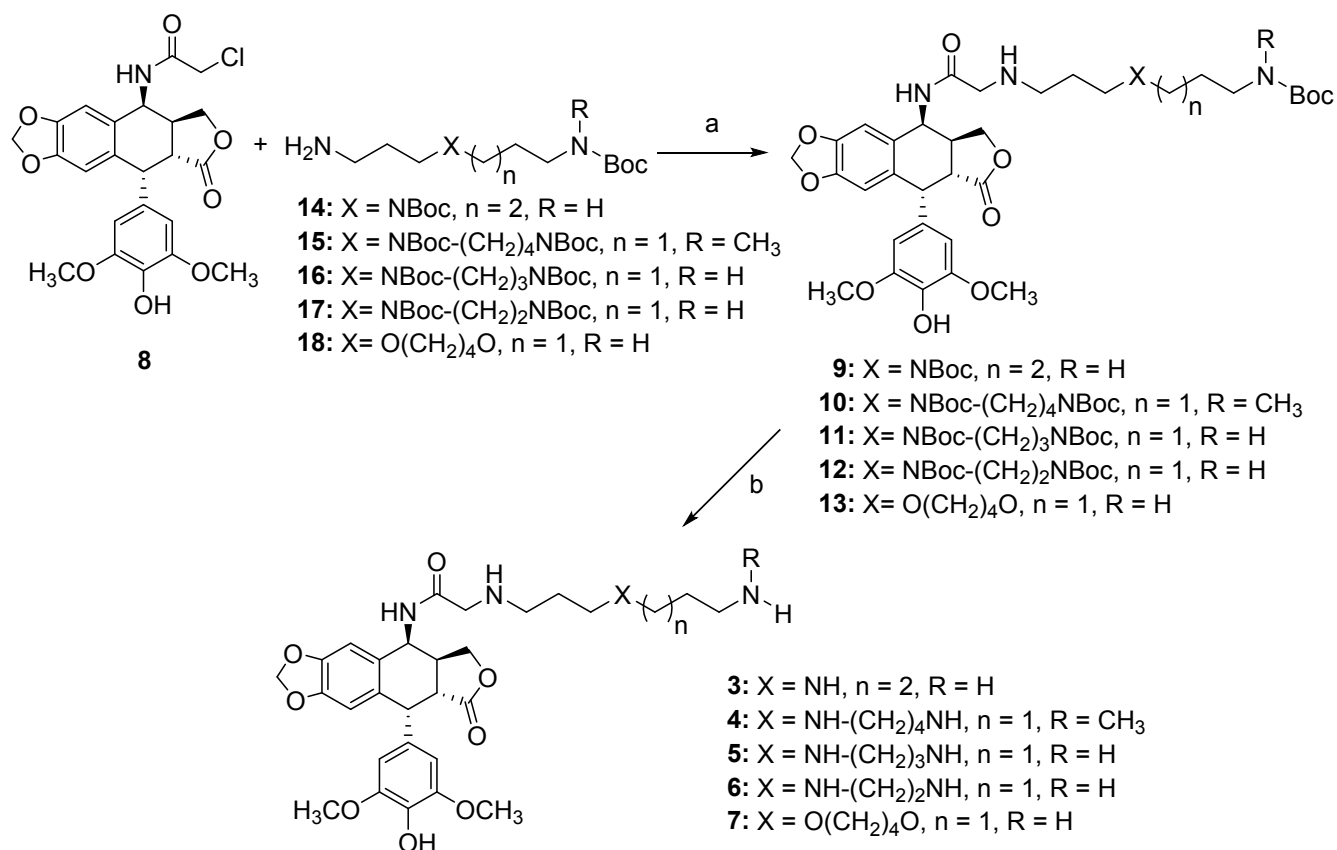
ctDNA binding assay. The UV spectrum (250-350nm) of the selected compounds was recorded (*Perkin Elmer* spectrophotometer) at 50µM in 10mM Tris 50mM KCl buffer. Then, each compound was titrated with ctDNA (calf thymus DNA, *Sigma*). The UV absorbance contribution of ctDNA in the selected range was compensated by adding the same amount of DNA in the sample and reference cells. The spectra were recorded and the variation of the absorbance at 290nm caused by a four-fold excess of ctDNA was considered for DNA binding evaluation.

Chemistry

General Considerations. All reactions were performed with dry glassware under atmosphere of nitrogen otherwise noted. Melting points were taken in glass capillary tubes on a Buchi SMP-20 apparatus and are uncorrected. ^1H and ^{13}C NMR spectra were recorded on Varian VXR 400 spectrometer in CDCl_3 , D_2O , $\text{DMSO}-d_6$ or CD_3OD as solvents. Chemical shifts (δ) are given in ppm from tetramethylsilane with the solvent resonance as internal standard (CDCl_3 : δ 7.26, DMSO : δ 2.50, D_2O : δ 4.79, CD_3OD : δ 3.31 for ^1H -NMR and CDCl_3 : δ 77.16, DMSO : δ 39.52, CD_3OD : δ 49.00 for ^{13}C -NMR). For ^1H -NMR, data are reported as follows: chemical shift, multiplicity (s = singlet, d = doublet, dd = double of doublets, t = triplet, q = quartet, m = multiplet, br s = broad singlet), coupling constants (Hz) and integration. Electron spray ionization (ESI) mass spectra were recorded on VG 7070E instrument. Chromatographic separations were performed on silica gel columns by flash (Kieselgel 40, 0.040-0.063 mm; Merck), or gravity column (Kieselgel 60, 0.063-0.200 mm; Merck) chromatography. Reactions were followed by thin-layer chromatography (TLC) on Merck (0.25 mm) glass-packed pre-coated silica gel plates (60 F254) that were visualized in an iodine chamber, UV lamp, KMnO_4 and bromocresol green. The term “dried” refers to the use of anhydrous sodium sulphate. All the names were attributed by Chem BioDraw Ultra 14.0.

The new compounds **3-7** were synthesized as hydrochloride salts as reported in Scheme S1 by coupling the common intermediate 4-chloroacetamido-4-deoxy-4'-demethyl-epipodophyllotoxin (**8**) with the appropriate *N*-Boc protected polyamine (**14-18**), followed by acidic deprotection of the resulting intermediate **9-13**. The reference compound **F14512 (2)** was synthesized following the same synthetic procedure by coupling the intermediate **8** with *N*¹,*N*²,*N*³-tri-Boc-spermine.

*N*¹,*N*⁵-bis-Boc-spermidine (**14**) and *N*¹,*N*²,*N*³-tri-Boc-*N*¹-methylspermine (**15**) were prepared according to the procedures reported in Scheme S2 and Scheme S3, respectively. The *N*-Boc-protected polyamines **16-18** were synthesized according to literature procedures.^{1,2}



Scheme S1. (a) DMF/CH₃CN, Et₃N, KI, r.t., overnight, 24-67% yield; (b) CH₂Cl₂, HCl 4M in dioxane, 0°C, 2-4 hours, 33-82% yield. Boc = (CH₃)₃COCO.

2-chloro-*N*-((5*S*,5*aS*,8*aR*,9*R*)-9-(4-hydroxy-3,5-dimethoxyphenyl)-8-oxo-5,5*a*,6,8,8*a*,9-hexahydrofuro[3',4':6,7]naphtho[2,3-*d*][1,3]dioxol-5-yl)acetamide (8)

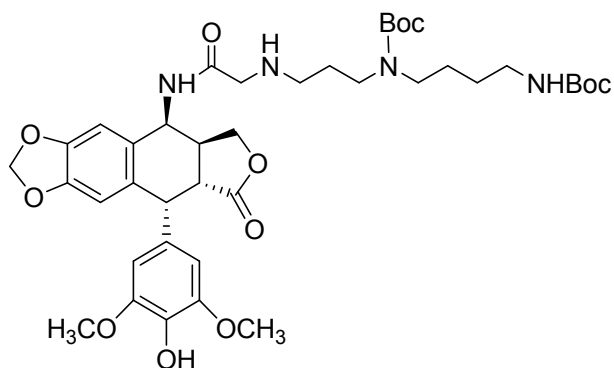
Compound **8** was synthesized according to the methodology previously published,³ and all data were in full agreement with that previously published.

¹H NMR (400 MHz, DMSO-*d*₆) δ 8.66 (d, *J* = 8.4 Hz, 1 H, D₂O exch), 8.27 (s, 1H, D₂O exch), 6.78 (s, 1H), 6.55 (s, 1H), 6.24 (s, 2H), 6.00 (d, *J* = 11.2 Hz, 2H), 5.17 (dd, *J* = 4.6 Hz, *J*' = 7.4 Hz, 1H), 4.51 (d, *J* = 4.8 Hz, 1H), 4.29 (t, *J* = 7.6 Hz, 1H), 4.10 (s, 2H), 3.81-3.76 (m, 1H), 3.63 (s, 6H), 3.15 (dd, *J* = 4.8 Hz, *J*' = 14.4 Hz, 1H), 3.02-2.94 (m, 1H).

General procedure for the synthesis of intermediates 9-13

To a solution of **8** (1 eq) in a mixture of CH₃CN (1,5 mL) and DMF (0.15 mL) were added Et₃N (2.5 eq) and then a spatula tip of KI. A solution of the appropriate N-Boc protected polyamines (**14-18**) (1-2.5 eq) in CH₃CN (0.5 mL) was then added with stirring at r.t. Stirring was maintained for 16 h, then the reaction medium was evaporated to give the crude products **9-13**, further purified by gravity column chromatography.

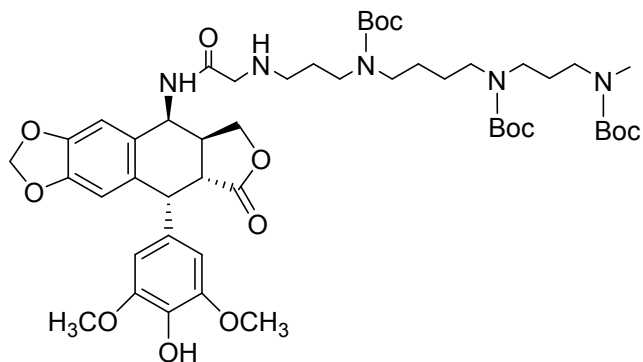
Tert-butyl(4-((tert-butoxycarbonyl)amino)butyl)(3-((2-(((5S,5aS,8aR,9R)-9-(4-hydroxy-3,5-dimethoxyphenyl)-8-oxo-5,5a,6,8,8a,9-hexahydrofuro[3',4':6,7]naphtho[2,3-d][1,3]dioxol-5-yl)amino)-2-oxoethyl)amino)propyl)carbamate (9)



Compound **9** was synthesized from **8** (50 mg, 0.105 mmol) and **14** (91 mg, 0.263 mmol). It was purified by silica gel chromatography eluted with petroleum ether:CH₂Cl₂:MeOH (5:3.3:1.7) affording a yellow oil (55 mg, 67 % yield).

¹H NMR (400 MHz, CDCl₃) δ 6.65 (s, 1H), 6.42 (s, 1H), 6.21 (s, 2H), 5.87 (s, 2H), 5.17 (d, *J* = 6.8Hz, 1H), 4.77 (br s, 1H), 4.48-4.45 (m, 1H), 4.31-4.28 (m, 1H), 3.76-3.73 (m, 1H), 3.66 (s, 6H), 3.23 (s, 2H), 3.11-3.00 (m, 7H), 2.89-2.83 (m, 1H), 2.54-2.41 (m, 2H), 1.57-1.54 (m, 2H), 1.43-1.40 (m, 2H), 1.33 (s, 9H+2H), 1.32 (s, 9H).

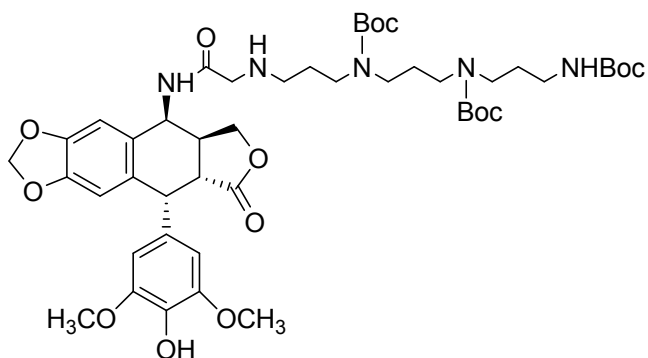
Tert-butyl(4-((tert-butoxycarbonyl)(3-((tert-butoxycarbonyl)(methyl)amino)propyl)amino)butyl)(3-((2-(((5S,5aS,8aR,9R)-9-(4-hydroxy-3,5-dimethoxyphenyl)-8-oxo-5,5a,6,8,8a,9-hexahydrofuro[3',4':6,7]naphtho[2,3-d][1,3]dioxol-5-yl)amino)-2-oxoethyl)amino)propyl)carbamate (10)



Compound **10** was synthesized from **8** (21 mg, 0.043 mmol) and **15** (22.5 mg, 0.043 mmol). It was purified by silica gel chromatography eluted with petroleum ether:CH₂Cl₂:MeOH: aq 33% NH₄OH (5:4.3:0.7:0.02) affording a yellow oil (17 mg, 41 % yield).

¹H NMR (400 MHz, CDCl₃) δ 6.71 (s, 1H), 6.51 (s, 1H), 6.28 (s, 2H), 5.95 (s, 2H), 5.25 (d, *J* = 4.4 Hz, 1H), 4.58 (d, *J* = 3.6 Hz, 1H), 4.40-4.36 (m, 1H), 3.84-3.80 (m, 1H), 3.76 (s, 6H), 3.32 (s, 2H), 3.18-3.15 (m, 10H), 2.96- 2.94 (m, 2H), 2.82 (s, 3H), 2.64-2.50 (m, 2H), 1.73-1.70 (m, 2H), 1.66-1.60 (m, 6H), 1.43 (s, 18H), 1.40 (s, 9H).

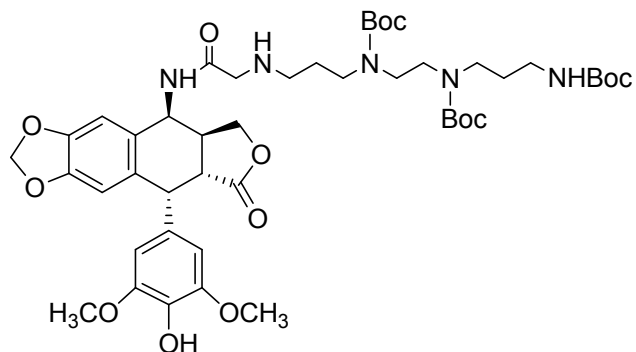
***Tert*-butyl(3-((*tert*-butoxycarbonyl)(3-((*tert*-butoxycarbonyl)amino)propyl)amino)propyl)(3-((2-(((5*S*,5*aS*,8*aR*,9*R*)-9-(4-hydroxy-3,5-dimethoxyphenyl)-8-oxo-5,5*a*,6,8,8*a*,9-hexahydrofuro[3',4':6,7]naphto[2,3-*d*][1,3]dioxol-5-yl)amino)-2-oxoethyl)amino)propyl)carbamate (**11**)**



Compound **11** was synthesized from **8** (50 mg, 0.105 mmol) and **16** (128 mg, 0.263 mmol). It was purified by silica gel chromatography eluted with petroleum ether:CH₂Cl₂:MeOH: aq 33% NH₄OH (5:4.3:0.7:0.02) affording a yellow oil (60 mg, 62 % yield).

¹H NMR (400 MHz, CDCl₃) δ 6.66 (s, 1H), 6.44 (s, 1H), 6.22 (s, 2H), 5.89 (s, 2H), 5.19 (d, *J* = 6.8 Hz, 1H), 4.53-4.46 (m, 1H), 4.32-4.29 (m, 1H), 3.79-3.70 (m, 1H), 3.68 (s, 6H), 3.25 (s, 2H), 3.21-3.09 (m, 5H), 3.05-3.03 (m, 7H), 2.52-2.45 (m, 2H), 1.64-1.57 (m, 6H), 1.37 (s, 9H), 1.35 (s, 9H), 1.34 (s, 9H).

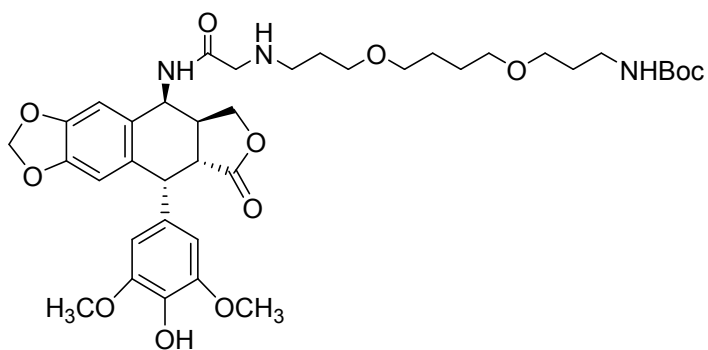
***Tert*-butyl(2-((*tert*-butoxycarbonyl)(3-((*tert*-butoxycarbonyl)amino)propyl)amino)ethyl)(3-((2-(((5*S*,5*aS*,8*aR*,9*R*)-9-(4-hydroxy-3,5-dimethoxyphenyl)-8-oxo-5,5*a*,6,8,8*a*,9-hexahydrofuro[3',4':6,7]naphto[2,3-*d*][1,3]dioxol-5-yl)amino)-2-oxoethyl)amino)propyl)carbamate (12)**



Compound **12** was synthesized from **8** (100 mg, 0.210 mmol) and **17** (249 mg, 0.525 mmol). It was purified by silica gel chromatography eluted with petroleum ether:CH₂Cl₂:MeOH: aq 33% NH₄OH (5:4.3:0.7:0.02) affording a yellow oil (45 mg, 24% yield).

¹H NMR (400 MHz, CDCl₃) δ 6.71 (s, 1H), 6.49 (s, 1H), 6.28 (s, 2H), 5.95 (s, 2H), 5.26-5.20 (m, 1H), 4.60-4.53 (m, 1H), 4.38-4.36 (m, 1H), 3.82-3.81 (m, 1H), 3.74 (s, 6H), 3.35-3.27 (m, 3H), 3.27-3.16 (m, 8H), 3.11-3.03 (m, 2H), 3.02-2.96 (m, 1H), 2.62-2.51 (m, 2H), 1.72-1.55 (m, 4H), 1.43 (s, 9H), 1.41 (s, 18H).

***Tert*-butyl(3-(4-(3-((2-(((5*S*,5*aS*,8*aR*,9*R*)-9-(4-hydroxy-3,5-dimethoxyphenyl)-8-oxo-5,5*a*,6,8,8*a*,9-hexahydrofuro[3',4':6,7]naphto[2,3-*d*][1,3]dioxol-5-yl)amino)-2-oxoethyl)amino)propoxy) butoxy)propyl)carbamate (13)**



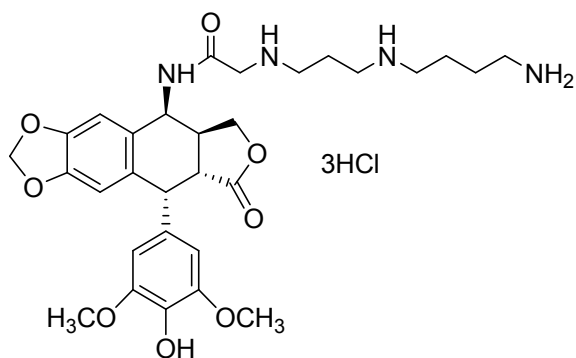
Compound **13** was synthesized from **8** (70 mg, 0.147 mmol) and **18** (112 mg, 0.368 mmol). It was purified by silica gel chromatography eluted with petroleum ether:CH₂Cl₂:MeOH: aq 33% NH₄OH (5:4.3:0.7:0.02) affording a yellow oil (44 mg, 40% yield).

¹H NMR (400 MHz, CDCl₃) δ 7.69 (br s, 1H), 6.72 (s, 1H), 6.52 (s, 1H), 6.29 (s, 2H), 5.97 (s, 2H), 5.23 (dd, *J* = 4.0 Hz, *J'* = 8.0 Hz, 1H), 4.58 (d, *J* = 3.6 Hz, 1H), 4.40-4.37 (m, 1H), 3.84-3.78 (m, 1H), 3.76 (s, 6H), 3.47-3.37 (m, 10H), 3.21-3.19 (m, 2H), 2.94-2.93 (m, 2H), 2.72 (t, *J* = 5.8 Hz, 2H), 1.75-1.70 (m, 4H), 1.66-1.55 (m, 4H), 1.42 (s, 9H).

General procedure for the synthesis of compounds 3-7

To a cooled solution (0 °C) of the appropriate intermediate (**9-13**) (1 eq) in CH₂Cl₂ (0.5 mL) a solution of 4M HCl in dioxane (0.8 mL) was added. After 2-4 hours, the solvents were removed and the residue was washed with Et₂O to provide the final compounds **3-7** as hydrochloride salts.

2-((3-((4-aminobutyl)amino)propyl)amino)-*N*-((5*S*,5*aS*,8*aR*,9*R*)-9-(4-hydroxy-3,5-dimethoxyphenyl)-8-oxo-5,5*a*,6,8,8*a*,9-hexahydrofuro[3',4':6,7]naphtho[2,3-*d*][1,3]dioxol-5-yl)acetamide trihydrochloride (**3**)



Compound **3** was synthesized from **9** (60.5 mg, 0.077 mmol): yellow solid (36 mg, 68 % yield);

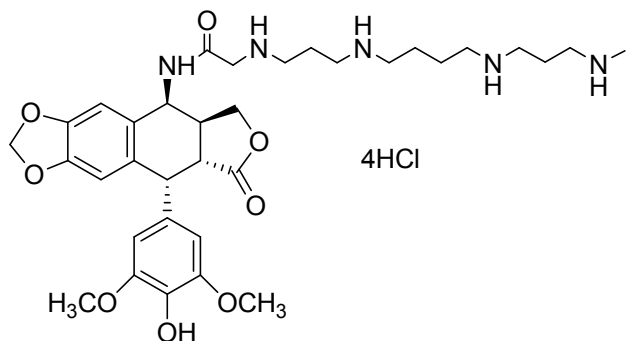
m.p.: 195 °C.

¹H NMR (400 MHz, DMSO-*d*₆) δ 8.98 (br s, 1H, D₂O exch), 8.26 (br s, 2H, D₂O exch), 6.80 (s, 1H), 6.54 (s, 1H), 6.24 (s, 2H), 6.00 (d, *J* = 10.8 Hz, 2H), 5.22 (dd, *J* = 4.4 Hz, *J'* = 8.0 Hz, 1H), 4.51 (d, *J* = 4.8 Hz, 1H), 4.27 (t, *J* = 7.8 Hz, 1H), 3.96-3.87 (m, 1H), 3.71 (s, 2H), 3.63 (s, 6H), 3.23 (dd, *J* = 5.4 Hz, *J'* = 14.6 Hz, 2H), 3.06-2.93 (m, 6H), 2.83-2.75 (m, 2H), 2.09-1.95 (m, 2H), 1.76-1.57 (m, 4H).

¹³C NMR (100 MHz, DMSO-*d*₆) δ 174.47, 165.09, 147.80, 147.16, 146.52, 134.92, 132.43, 130.22, 129.58, 109.52, 108.88, 108.60, 101.35, 68.40, 56.19, 47.70, 47.06, 45.85, 44.28, 43.95, 42.72, 38.03, 24.51, 23.87, 22.66.

MS (ESI⁺): *m/z* 585 [M+1]⁺.

***N*-((5*S*,5*aS*,8*aR*,9*R*)-9-(4-hydroxy-3,5-dimethoxyphenyl)-8-oxo-5,5*a*,6,8,8*a*,9-hexahydrofuro [3',4':6,7]naphtho[2,3-*d*][1,3]dioxol-5-yl)-2,6,11,15-tetraazaheptadecan-17-amide tetrahydrochloride (4)**



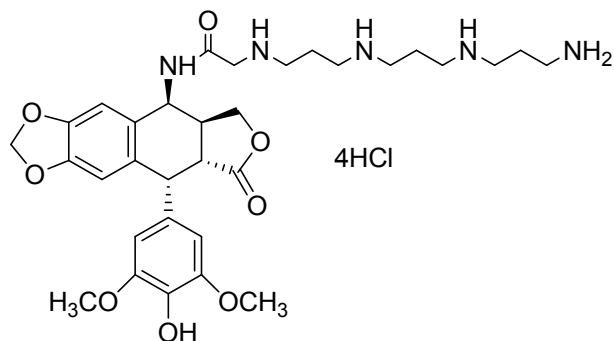
Compound **4** was synthesized from **10** (17 mg, 0.017 mmol): white solid (4.8 mg, 33 % yield); **m.p.:** 220°C.

¹H NMR (400 MHz, D₂O) δ 6.86 (s, 1H), 6.53 (s, 1H), 6.41 (s, 2H), 5.97 (s, 1H), 5.92 (s, 1H), 5.27 (d, *J* = 3.2 Hz, 1H), 4.64 (d, *J* = 4.8 Hz, 1H), 4.49-4.43 (m, 1H), 4.01-3.91 (m, 3H), 3.74 (s, 6H), 3.27-3.06 (m, 14H), 2.74 (s, 3H), 2.19-2.10 (m, 4H), 1.79-1.77 (m, 4H).

¹³C NMR (100 MHz, D₂O) δ 177.85, 165.39, 148.02, 147.37, 147.05, 133.35, 132.02, 131.72, 127.79, 109.46, 109.18, 108.50, 101.60, 69.85, 56.15, 48.28, 47.96, 45.69, 44.72, 44.33, 42.72, 41.46, 36.86, 32.93, 22.76, 22.47, 22.18.

MS (ESI⁺): *m/z* 656 [M+1]⁺.

2-((3-((3-((3-aminopropyl)amino)propyl)amino)propyl)amino)-*N*-((5*S*,5*aS*,8*aR*,9*R*)-9-(4-hydroxy-3,5-dimethoxyphenyl)-8-oxo-5,5*a*,6,8,8*a*,9-hexahydrofuro[3',4':6,7]naphtho[2,3-*d*][1,3]dioxol-5-yl)acetamide tetrahydrochloride (5)



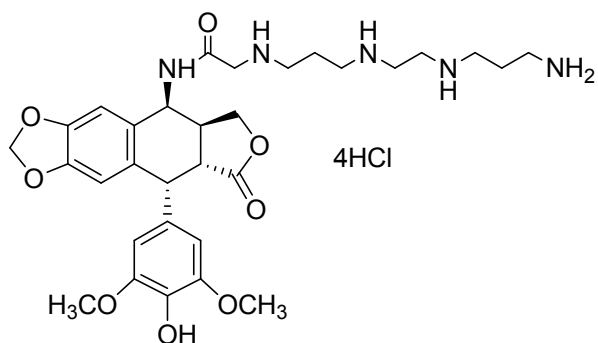
Compound **5** was synthesized from **11** (61.5 mg, 0.066 mmol): white solid (35 mg, 68 % yield); **m.p.:** 215°C.

¹H NMR (400 MHz, DMSO-*d*₆) δ 9.34 (br s, 5H, D₂O exch), 9.06 (br s, 1H, D₂O exch), 8.27 (br s, 2H, D₂O exch), 8.15 (br s, 2H, D₂O exch), 6.81 (s, 1H), 6.55 (s, 1H), 6.24 (s, 2H), 6.01 (d, *J* = 12.4 Hz, 2H), 5.28-5.19 (m, 1H), 4.57-4.47 (m, 1H), 4.34-4.21 (m, 1H), 4.02-3.87 (m, 1H), 3.79 (s, 2H), 3.63 (s, 6H), 3.26-3.15 (m, 1H), 3.14-2.80 (m, 13H), 2.17-1.84 (m, 6H).

¹³C NMR (100 MHz, CD₃OD) δ 177.10, 165.95, 149.91, 148.93, 148.64, 135.78, 133.89, 131.63, 130.06, 110.85, 110.23, 109.59, 102.80, 70.17, 56.77, 45.88, 45.51, 45.24, 44.86, 42.35, 38.81, 37.82, 25.33, 24.04, 23.42.

MS (ESI⁺): *m/z* 628 [M+1]⁺.

2-((3-((2-((3-aminopropyl)amino)ethyl)amino)propyl)amino)-*N*-((5*S*,5*aS*,8*aR*,9*R*)-9-(4-hydroxy-3,5-dimethoxyphenyl)-8-oxo-5,5*a*,6,8,8*a*,9-hexahydrofuro[3',4':6,7]naphtho[2,3-*d*][1,3]dioxol-5-yl)acetamide tetrahydrochloride (6)



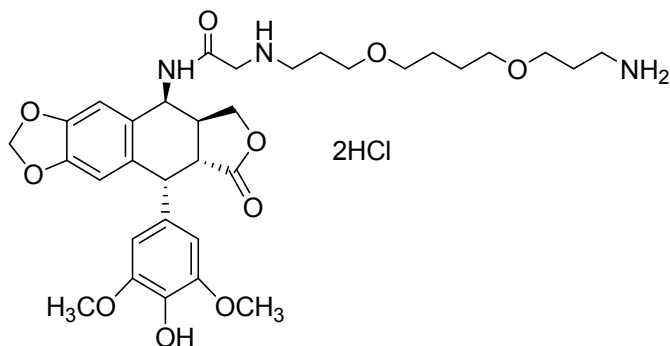
Compound **6** was synthesized from **12** (45 mg, 0.049 mmol): white solid (35 mg, 82 % yield); **m.p.:** 190°C.

¹H NMR (400 MHz, DMSO-*d*₆) δ 9.76 (br s, 3H, D₂O exch), 9.25 (br s, 2H, D₂O exch), 9.04 (d, *J* = 8.0 Hz, 1H, D₂O exch), 8.27 (br s, 1H, D₂O exch), 8.11 (br s, 3H, D₂O exch), 6.80 (s, 1H), 6.55 (s, 1H), 6.24 (s, 2H), 6.01 (d, *J* = 12.0 Hz, 2H), 5.23 (dd, *J* = 4.4 Hz, , *J*' = 8.4 Hz, 1H), 4.52 (d, *J* = 5.2 Hz, 1H), 4.28 (t, *J* = 7.8 Hz, 1H), 3.96-3.92 (m, 1H), 3.80 (s, 2H), 3.63 (s, 6H), 3.47-3.35 (m, 5H), 3.20 (dd, *J* = 5.2 Hz, , *J*' = 14.4 Hz, 1H), 3.12-2.91 (m, 8H), 2.14-1.95 (m, 4H).

¹³C NMR (100 MHz, DMSO-*d*₆) δ 174.20, 164.99, 147.68, 147.01, 146.65, 134.90, 132.24, 130.00, 129.63, 109.36, 108.99, 108.33, 101.12, 68.08, 66.14, 65.10, 55.98, 47.81, 47.14, 44.17, 43.87, 42.51, 41.20, 36.00, 23.90, 22.27, 15.06.

MS (ESI⁺): *m/z* 614 [M+1]⁺.

2-((3-(4-(3-aminopropoxy)butoxy)propyl)amino)-N-((5S,5aS,8aR,9R)-9-(4-hydroxy-3,5-dimethoxyphenyl)-8-oxo-5,5a,6,8,8a,9-hexahydrofuro[3',4':6,7]naphtho[2,3-d][1,3]dioxol-5-yl)acetamide dihydrochloride (7)

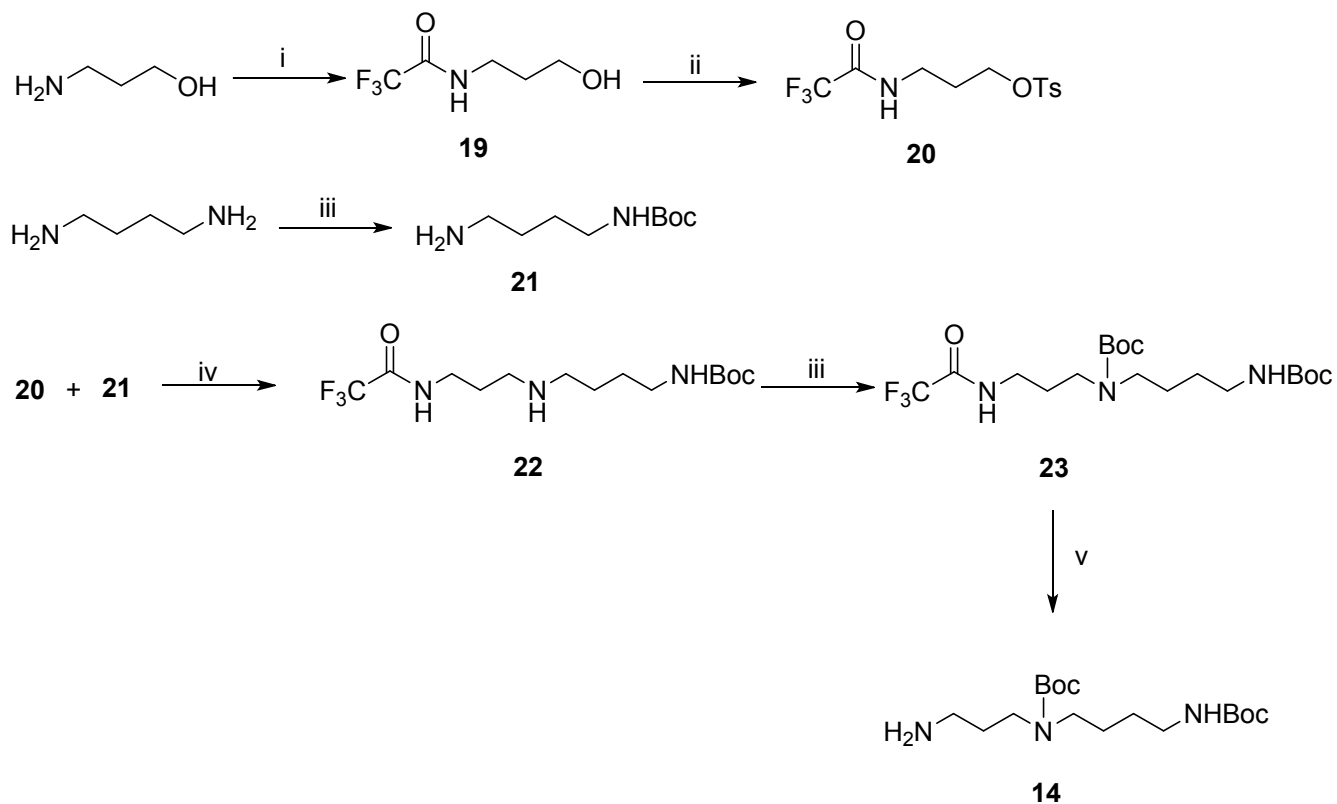


Compound **7** was synthesized from **13** (44 mg, 0.059 mmol): white solid (34 mg, 78 % yield); m.p.: 190 °C.

¹H NMR (400 MHz, DMSO-*d*₆) δ 9.03 (d, *J* = 8.4 Hz, 1H, D₂O exch), 8.27 (br s, 1H, D₂O exch), 6.79 (s, 1H), 6.56 (s, 1H), 6.25 (s, 2H), 6.01 (d, *J* = 12.8 Hz, 2H), 5.23 (dd, *J* = 4.6 Hz, *J*' = 8.6 Hz, 1H), 4.52 (d, *J* = 5.2 Hz, 1H), 4.28 (t, *J* = 8.0 Hz, 1H), 3.94-3.89 (m, 1H), 3.77 (s, 2H), 3.63 (s, 6H), 3.46-3.42 (m, 4H), 3.37-3.36 (m, 4H), 3.23 (dd, *J* = 5.2 Hz, *J*' = 14.4 Hz, 1H), 3.17 (d, *J* = 4.4 Hz, 1H), 3.05-2.93 (m, 2H), 2.81 (t, *J* = 7.4 Hz, 2H), 1.92-1.74 (m, 4H), 1.58-1.46 (m, 4H).

¹³C NMR (100 MHz, DMSO-*d*₆) δ 174.20, 165.48, 147.70, 147.33, 146.73, 134.89, 132.41, 130.21, 129.84, 109.59, 108.96, 108.30, 101.15, 70.20, 69.91, 68.36, 67.06, 56.17, 54.89, 48.94, 48.02, 47.10, 44.90, 42.71, 36.73, 28.97, 27.44, 26.11.

MS (ESI⁺): m/z 644 [M+1]⁺.



Scheme S2. (i) CF_3COOEt , 4h, r.t., 81% yield; (ii) TsCl , CH_2Cl_2 ; Et_3N , DMAP, 45 min, r.t., 68% yield; (iii) Boc_2O , CH_2Cl_2 , 16h, r.t., 86% yield; (iv) THF, Et_3N , 5 d, r.t., 35% yield; (v) NaOH 40% p/p, MeOH, 16h, r.t., 46% yield; Boc = $(\text{CH}_3)_3\text{COCO}$.

2,2,2-trifluoro-N-(3-hydroxypropyl)acetamide (**19**)

To 3-amino-1-propanol (2 g, 0.026 mol), ethyltrifluoroacetate (5.82 g, 0.037 mol) was added at 0 °C. The stirring was maintained for 4 h at r.t. The solvent was removed under vacuum to give **19** as a colorless oil (81% yield). $^1\text{H NMR}$ (400 MHz, CDCl_3) δ 8.74 (br s, 1H, D_2O exch), 3.52 (t, $J = 4.8$ Hz, 2H), 3.69 (br s, 1H, D_2O exch), 3.18 (t, $J = 5.1$ Hz, 2H), 1.78-1.70 (m, 2H).

3-(2,2,2-trifluoroacetamido)propyl 4-methylbenzenesulfonate (**20**)

To a cooled solution (0 °C) of **19** (3.66 g, 0.021 mol) in CH_2Cl_2 (20 mL), Et_3N (2.43 g, 0.024 mol), a catalytic amount of DMAP and tosyl chloride (4.06 g, 0.021 mol) were added at 0 °C. The reaction mixture was stirred at r.t. for 45 min. Removal of the solvent under vacuum

gave a residue that was purified by flash column chromatography eluted with EtOAc/petroleum ether (8:2), providing **20** as a white solid (68% yield). **¹H NMR** (400 MHz, CDCl₃) δ 7.80-7.78 (m, 2H), 7.38-7.36 (m, 2H), 4.11 (t, *J* = 5.6 Hz, 2H), 3.50-3.45 (m, 2H), 2.46 (s, 3H), 2.00-1.94 (m, 2H).

***Tert*-butyl (4-aminobutyl)carbamate (21)**

To a solution of 1,4-butanediamine (2 g, 0.023 mol) in CH₂Cl₂ (30 mL), a solution of Boc₂O (1 g, 0.005 mol) in CH₂Cl₂ (30 mL) was slowly added in 20 min. Stirring was continued for 16 h at r.t., then the solvent was removed under vacuum and the crude product was purified by flash column chromatography eluted with CH₂Cl₂:MeOH:aq 33% NH₄OH (8:2:0.2) to afford **21** as a yellow oil (86% yield). **¹H NMR** (400 MHz, CDCl₃) δ 5.95 (br s, 1H, D₂O exch), 3.24-3.19 (m, 2H), 2.79-2.72 (m, 2H), 2.34 (br s, 2H, D₂O exch), 1.59-1.52 (m, 4H), 1.38 (s, 9H).

***Tert*-butyl(4-((3-(2,2,2-trifluoroacetamido)propyl)amino)butyl)carbamate (22)**

To a cooled solution (0 °C) of **20** (1.06 g, 0.003 mol) in THF (4 mL), a solution of **21** (0.740 g, 0.004 mol) in THF (4 mL) followed by Et₃N (0.33 g, 0.003 mol) was added. The reaction mixture was stirred for 5 days at r.t. Removal of the solvent gave a crude product that was purified by flash column chromatography eluted with CH₂Cl₂/MeOH/aq 33% NH₄OH (9:1:0.05), providing **22** as a yellow oil (35%). **¹H NMR** (400 MHz, CDCl₃) δ 4.64 (br s, 1H, D₂O exch), 3.48 (t, *J* = 6 Hz, 2H), 3.11-3.09 (m, 2H), 2.84 (t, *J* = 5.2 Hz, 2H), 2.63 (t, *J* = 6.4 Hz, 2H), 1.72-1.76 (m, 2H), 1.54-1.52 (m, 4H), 1.44 (s, 9H).

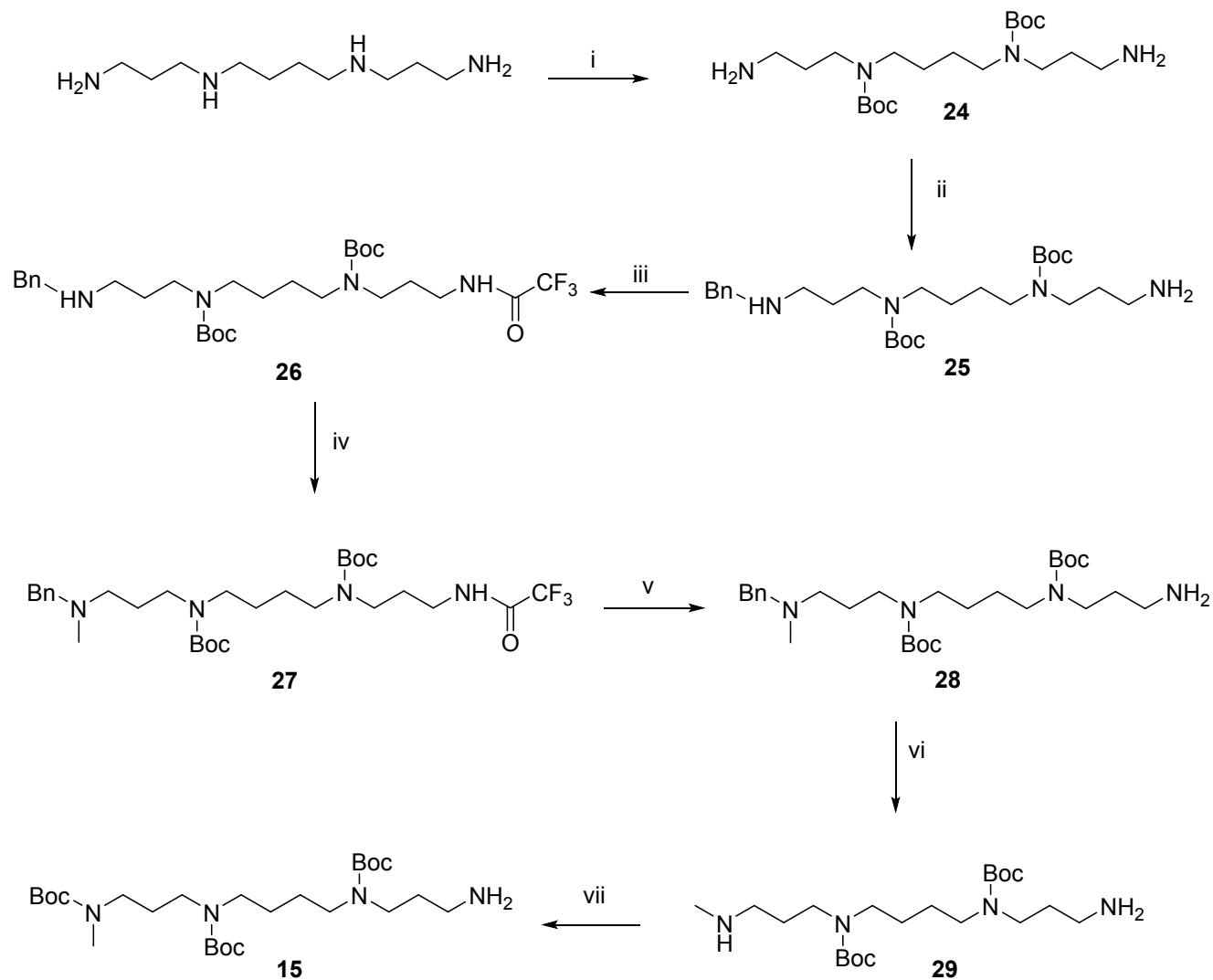
***Tert*-butyl(4-((*tert*-butoxycarbonyl)amino)butyl)(3-(2,2,2-trifluoroacetamido)propyl)carbamate (23)**

To a solution of **22** (430 mg, 1.259 mmol) in CH₂Cl₂ (4.5 mL) a solution of Boc₂O (462.22 mg, 2.12 mmol) in CH₂Cl₂ (4.5 mL) was added and stirring was continued for 16 h at r.t. The solvent was removed under vacuum to give **23** as a white oil used in the next step without further purification.

***Tert*-butyl (3-aminopropyl)(4-((*tert*-butoxycarbonyl)amino)butyl)carbamate (14)**

To a solution of **23** (970 mg, 2.00 mmol) in MeOH (4 mL), NaOH 40% p/p (2.08 mL) was added at 0 °C. The resulting mixture was stirred for 16 h at r.t. After removal of the solvent,

the residue was purified by flash column chromatography eluted with $\text{CH}_2\text{Cl}_2:\text{MeOH}:\text{aq } 33\% \text{NH}_4\text{OH}$ (9:1:0.2) to afford **14** as a yellow oil (46%). $^1\text{H NMR}$ (400 MHz, CDCl_3) δ 4.58 (br s, 1H, D_2O exch), 3.23-3.09 (m, 6H), 2.68-2.62 (m, 2H), 2.08-1.95 (m, 2H), 1.70-1.61 (m, 2H), 1.60-1.48 (m, 2H), 1.41 (s, 18H).



Scheme S3. (i) a) CF_3COOEt , MeOH, r.t., 1h; b) Boc_2O , MeOH, r.t., 16h; c) K_2CO_3 , pH = 11, reflux, 4h; 71% yield; (ii) a) benzaldehyde, toluene, reflux, 5h; b) NaBH_4 , EtOH, r.t., 12h, quant. yield; (iii) CF_3COOEt , r.t., 16h, 92% yield; (iv) MeI, Et_3N , THF, r.t., 24h, 30% yield; (v) NaOH 40% p/p, MeOH, r.t., 16 h, 92% yield; (vi) H_2/Pd , MeOH, r.t., 5h, 76% yield; (vii) a) CF_3COOEt , MeOH, -78°C , 30min; b) Boc_2O , MeOH, r.t., 16h; c) NaOH 40% p/p, r.t., 16h; 41% yield. Boc = $(\text{CH}_3)_3\text{COCO}$; Bn = $\text{CH}_2\text{C}_6\text{H}_5$.

Di-tert-butyl butane-1,4-diylbis((3-aminopropyl)carbamate) (24)

To a stirring solution of spermine (1 g, 4.942 mmol) in MeOH (20 mL), ethyltrifluoroacetate (1.40 g, 9.884 mmol) were added dropwise at -78 °C within 30 min. The stirring was continued for 3 h at r.t. and then a solution of Boc₂O (2.4 g, 10.87 mmol) in MeOH (1.2 mL) was added. Stirring was continued for 16 h at r.t., then K₂CO₃ was added until reaching pH =11 and the stirring was continued for 4 h under reflux. After evaporation of the solvent, the residue was dissolved in CH₂Cl₂ (20 mL) and extracted with H₂O (3 x 10 mL). The organic phase was dried, filtered and concentrated under vacuum. The crude product was purified by flash column chromatography eluted with CH₂Cl₂:MeOH:aq 33% NH₄OH (8:2:0.2) to afford **24** as a yellow oil (71% yield). **¹H NMR** (400 MHz, CDCl₃) δ 4.31-4.16 (m, 8H), 3.27-3.16 (m, 4H, D₂O exch), 2.84-2.79 (m, 4H), 1.82-1.76 (m, 4H), 1.50-1.47 (m, 4H), 1.43 (s, 18H).

Tert-butyl(4-((3-aminopropyl)(tert-butoxycarbonyl)amino)butyl)(3-(benzylamino)propyl) carbamate (25)

To a solution of **24** (930 mg, 2.310 mmol) in toluene (40 mL) was added benzaldehyde (49 mg, 0.461 mmol). The resulting mixture was refluxed for 5 h with Dean-Stark apparatus, then the reaction medium was evaporated and the residue was taken up with EtOH (20 mL) and NaBH₄ (52 mg, 1.386 mmol) was added. The solution was stirred for 12 h at r.t. and after evaporation of the solvent, the crude product was dissolved in CH₂Cl₂ (20 mL). The organic phase was washed with brine (10 mL) dried, filtered and concentrated. Purification by flash column chromatography eluted with CH₂Cl₂:MeOH:aq 33% NH₄OH (9:1:0.1) afforded **25** as a yellow oil (quantitative yield). **¹H NMR** (400 MHz, CDCl₃) δ 7.29- 7.27 (m, 5H), 3.75 (s, 2H), 3.22-3.13 (m, 8H), 2.66 (t, *J* = 6.6 Hz, 2H), 2.59 (t, *J* = 6.8 Hz, 2H), 1.78- 1.69 (m, 4H), 1.64-1.62 (m, 4H), 1.44 (s, 18H).

Tert-butyl (3-(benzylamino)propyl)(4-((tert-butoxycarbonyl)(3-(2,2,2-trifluoroacetamido)propyl) amino)butyl)carbamate (26)

To a stirring solution of **25** (220 mg, 0.446 mmol) in MeOH (10 mL), ethyltrifluoroacetate (63 mg, 0.446 mmol) was added at -78°C for 1 h. The stirring was continued for 16 h at r. t. The solvent was removed under vacuum and the crude product was purified by flash column chromatography eluted with CH₂Cl₂:MeOH:aq 33% NH₄OH (9:1:0.05) to afforded **26** as a yellow oil (92% yield). **¹H NMR** (400 MHz, CDCl₃) δ 7.30- 7.32 (m, 5H), 3.78 (s, 2H), 3.31-

3.11 (m, 10H), 2.62 (t, 2H, $J = 7.0$ Hz), 1.98 (br s, 1H), 1.70-1.67 (m, 4H), 1.48-1.46 (m, 4H), 1.44 (s, 18H).

Tert-butyl(3-(benzyl(methyl)amino)propyl)(4-((tert-butoxycarbonyl)(3-(2,2,2-trifluoroacetamido) propyl)amino)butyl)carbamate (27)

To a stirring solution of **26** (241 mg, 0.409 mmol) in THF (10 mL), Et₃N (49.71 mg, 0.491 mmol) and methyl iodide (87.15 mg, 0.614 mmol) were added and the mixture was stirred at r.t. for 24 h. The solvent was removed under vacuum and the crude product was purified by flash column chromatography eluted with CH₂Cl₂:MeOH:aq 33% NH₄OH (9:1:0.04), providing **27** as a yellow oil (30% yield). ¹H NMR (400 MHz, CDCl₃) δ 7.29-7.27 (m, 5H), 3.46 (s, 2H), 3.29-3.26 (m, 4H), 3.15-3.13 (m, 6H), 2.37-2.39 (m, 2H), 2.17 (s, 3H), 1.67-1.65 (m, 4H), 1.46-1.43 (m, 4H), 1.41 (s, 18H).

Tert-butyl(4-((3-aminopropyl)(tert-butoxycarbonyl)amino)butyl)(3-(benzyl(methyl)amino)propyl) carbamate (28)

27 (72 mg, 0.119 mmol) was dissolved in MeOH (10 mL) and a solution of NaOH 40% p/p (0.05 mL) was added. The resulting mixture was stirred for 16 h at r.t. After removal of the solvent under vacuum, the residue was dissolved in CH₂Cl₂ (15 mL) and then washed with H₂O (3 x 10 mL). The combined organic layers were dried, filtered and concentrated to provide **28** as a yellow solid (92% yield).

¹H NMR (400 MHz, CDCl₃) δ 7.27-7.21 (m, 5H), 3.44 (s, 2H), 3.15-3.12 (m, 4H), 3.03-3.00 (m, 4H), 2.75-2.73 (m, 2H), 2.33 (t, $J = 6.0$ Hz, 2H), 2.15 (s, 3H), 1.71-1.68 (m, 4H), 1.46-1.45 (m, 4H), 1.41 (s, 18H).

Tert-butyl(3-aminopropyl)(4-((tert-butoxycarbonyl)(3-(methylamino)propyl)amino)butyl) carbamate (29)

A solution of **28** (151 mg, 0.306 mmol) in MeOH (25 mL) was hydrogenated over 10% Pd on charcoal (0.03 g) under stirring for 4 h. After the consumption of the starting material, the solution was filtered on celite in order to remove the catalyst and dried under vacuum. The residue was purified by flash column chromatography eluted with CH₂Cl₂:MeOH:aq 33% NH₄OH (8:2:0.2) affording **29** as a yellow oil (76% yield). ¹H NMR (400 MHz, CDCl₃) δ 3.22-

3.14 (m, 8H), 2.66 (t, $J = 6.6$ Hz, 2H), 2.56-2.54 (m, 2H), 2.41(s, 3H), 1.94 (br s, 3H, D₂O exch), 1.66-1.64 (m, 2H), 1.63-1.60 (m, 2H), 1.47-1.45 (m, 4H), 1.42 (s, 18H).

Tert-butyl (4-((3-aminopropyl)(tert-butoxycarbonyl)amino)butyl)(3-((tert-butoxycarbonyl)(methyl)amino)propyl)carbamate (15)

To a stirring solution of **29** (35 mg, 0.084 mmol) in MeOH (5 mL), ethyltrifluoroacetate (14.6 mg, 0.084 mmol) was added dropwise at -78 °C. After 30 min a solution of Boc₂O (18.3 mg, 0.084 mmol) in MeOH (1 mL) was added and stirring was continued for 16 h at r.t. Then, NaOH 40% p/p (0.8 mL) was added and the stirring was continued for 16 h at r.t. After evaporation of the solvent, the residue was dissolved in CH₂Cl₂ (10 mL), washed with brine (5 mL), dried, filtered and concentrated. The crude product was purified by flash column chromatography eluted with CH₂Cl₂:MeOH:aq 33% NH₄OH (9:1:0.1) to afforded **15** as a yellow oil (41% yield). **¹H NMR** (400 MHz, CDCl₃) δ 3.19-3.17 (m, 10H), 2.83 (s, 3H), 2.65-2.58 (m, 4H, D₂O exch), 1.74-1.71 (m, 4H), 1.49-1.46 (m, 4H), 1.44 (s, 18H), 1.43 (s, 9H).

Tert-butyl(3-aminopropyl)(3-((tert-butoxycarbonyl)(3-((tert-butoxycarbonyl)amino)propyl)amino)propyl)carbamate (16) and ***Tert-butyl (3-aminopropyl)(2-((tert-butoxycarbonyl)(3-((tert-butoxycarbonyl)amino)propyl)amino)ethyl)carbamate (17)***

16 and **17** were synthesized according to the methodology previously published for spermine.¹

16: **¹H NMR** (400 MHz, CDCl₃) δ 3.24-3.09 (m, 10H), 2.74-2.68 (m, 2H), 2.20 (br s, 2H, D₂O exch), 1.75-1.64 (m, 6H), 1.44 (s, 9H), 1.42 (s, 18H).

17: **¹H NMR** (400 MHz, CDCl₃) δ 3.38-3.20 (m, 10H), 2.74-2.68 (m, 2H), 2.38 (br s, 2H, D₂O exch), 1.78-1.60 (m, 4H), 1.58 (s, 27H).

Tert-butyl (3-(4-(3-aminopropoxy)butoxy)propyl)carbamate (18)

18 was synthesized according to the procedure previously published,² and all data were in full agreement with that previously published.

2-((3-((4-((3-aminopropyl)amino)butyl)amino)propyl)amino)-N-((5S,5aS,8aR,9R)-9-(4-hydroxy-3,5-dimethoxyphenyl)-8-oxo-5,5a,6,8,8a,9-hexahydrofuro[3',4':6,7]naphtho[2,3-d][1,3]dioxol-5-yl)acetamide tetrahydrochloride (2, F14512)

The reference compound **F14512** was resynthesized by coupling intermediate **8** with N^1, N^2, N^3 -tri-Boc-spermine according to the procedure described for the synthesis of intermediates **9-13**. The obtained intermediate was then deprotected following the procedure described for the final compounds **3-7**.

$^1\text{H NMR}$ (400 MHz, $\text{DMSO-}d_6$) δ 9.32 (br s, 6H, D_2O exch), 9.11 (d, 1H, $J = 8.0$ Hz, D_2O exch), 8.28 (br s, 1H, D_2O exch), 8.19 (br s, 3H, D_2O exch), 6.81 (s, 1H), 6.55 (s, 1H), 6.24 (s, 2H), 6.01 (d, $J = 11.2$ Hz, 2H), 5.27-5.18 (m, 1H), 4.52 (d, $J = 4.0$ Hz, 1H), 4.32-4.22 (m, 1H), 3.98-3.94 (m, 1H), 3.79 (s, 2H), 3.63 (s, 6H), 3.24 (dd, $J = 4.4$ Hz, $J' = 14.4$ Hz 1H), 3.06-2.89 (m, 13H), 2.15-1.96 (m, 4H), 1.81-1.69 (m, 4H).

$^{13}\text{C NMR}$ (100 MHz, $\text{DMSO-}d_6$) δ 174.55, 165.06, 147.72, 147.42, 146.37, 135.04, 132.74, 130.45, 130.00, 109.48, 109.03, 108.60, 101.32, 56.62, 54.77, 47.36, 46.10, 44.32, 42.83, 36.62, 36.53, 24.67, 23.76, 22.90, 22.53.

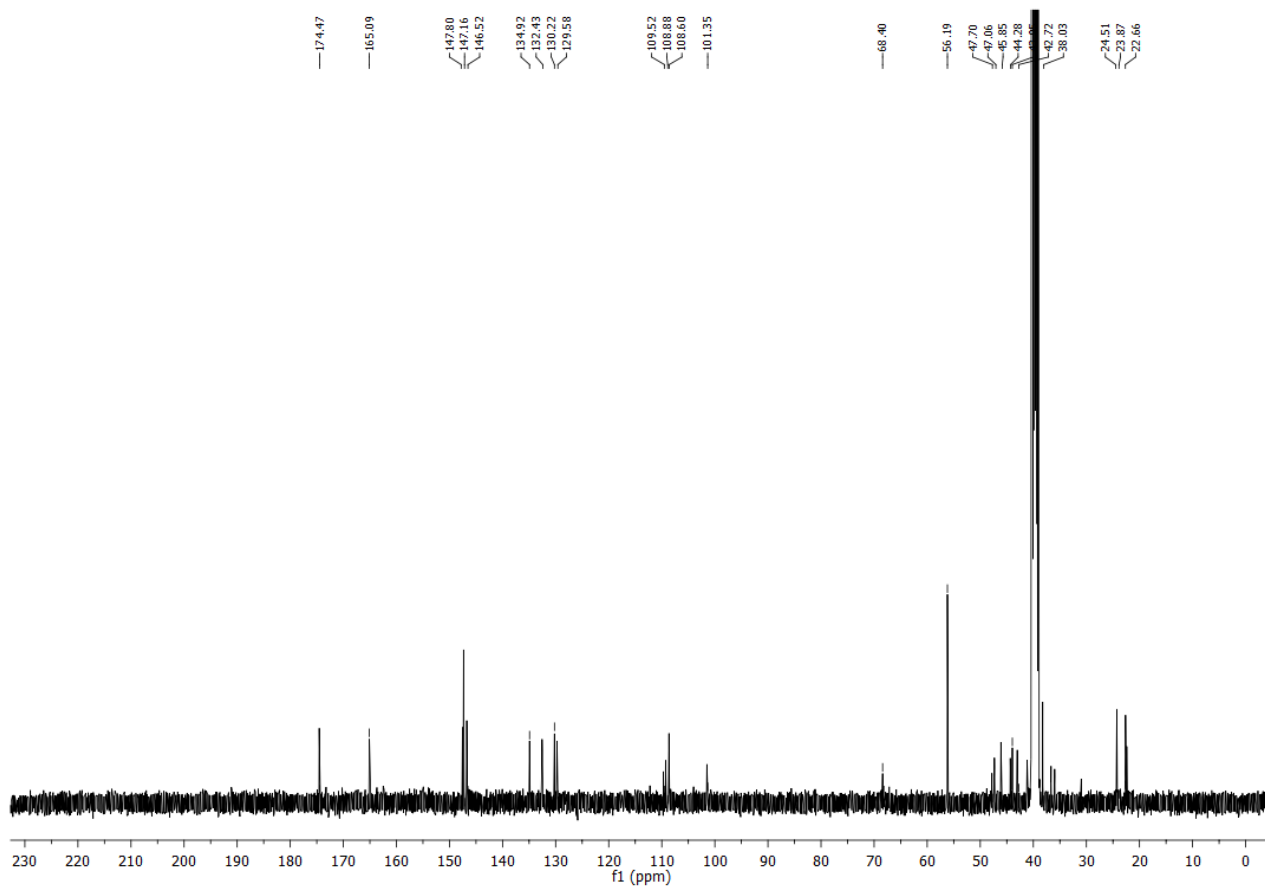
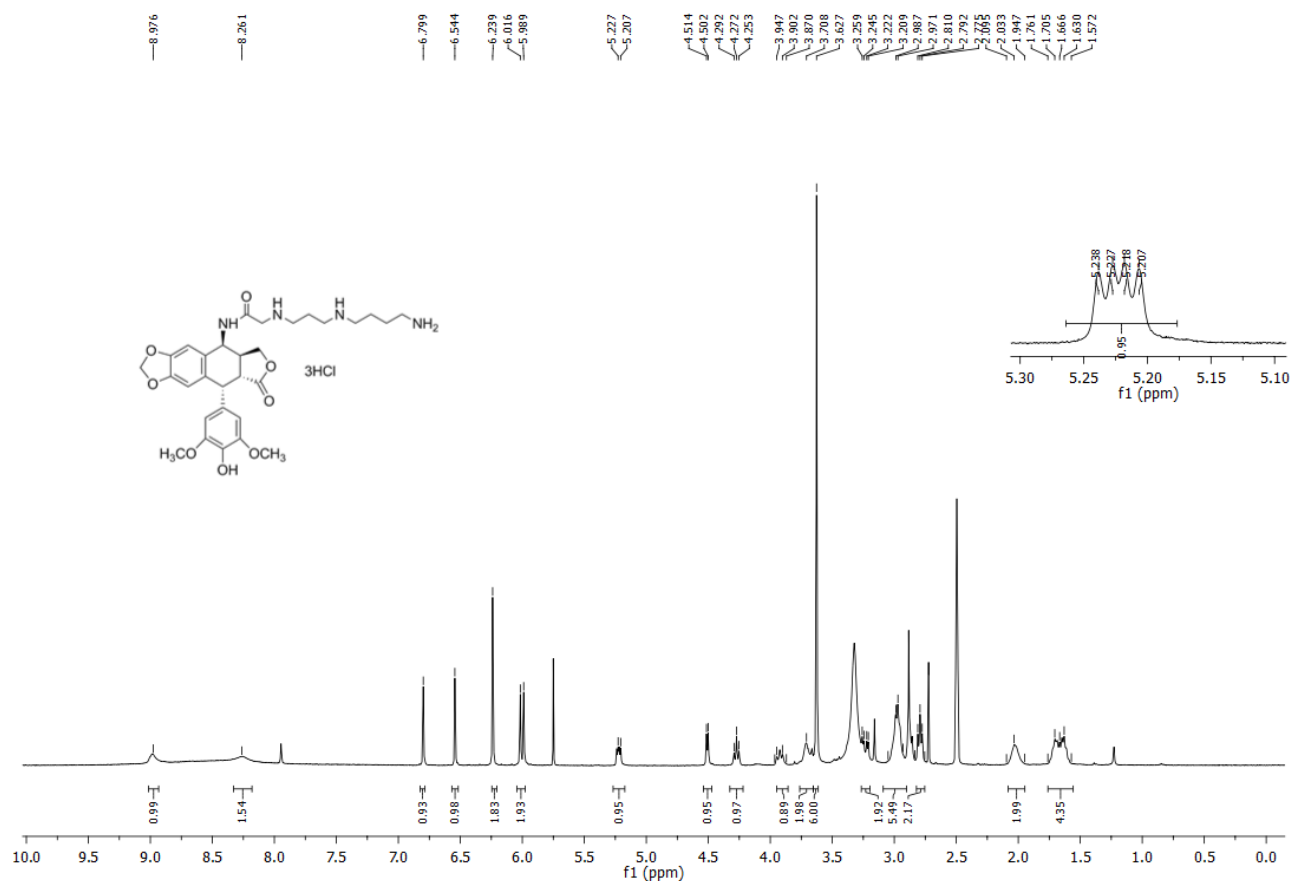
MS (ESI⁺): m/z 642 [M+1]⁺.

Mp: 220 °C

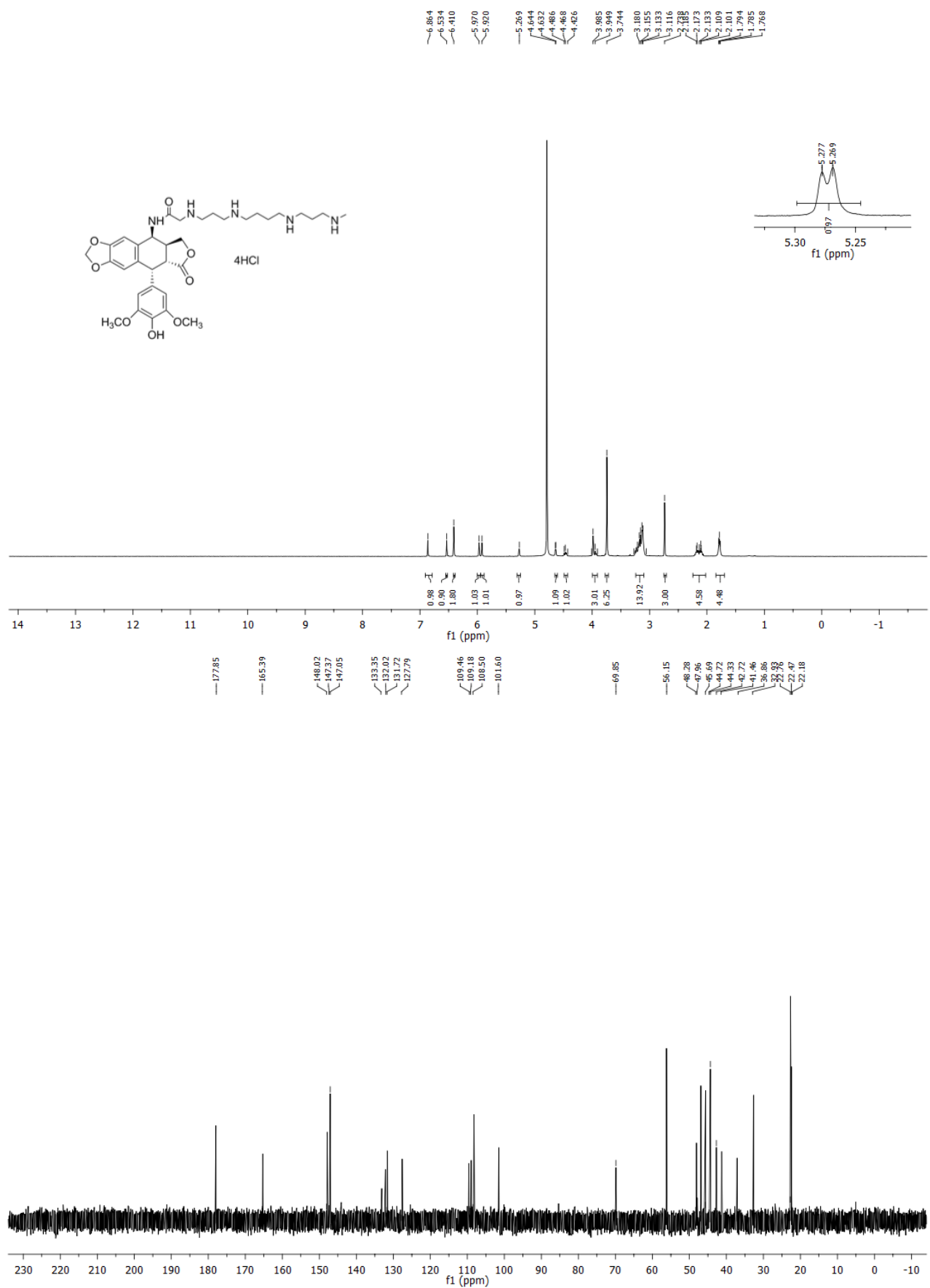
References

1. Wellendorph P.; Jaroszewski J.W.; Hansen S.H.; Franzyk H. *Eur J Med Chem* **2003**, *38*, 117.
2. Marom H.; Miller K.; Bechor-Bar Y.; Tsarfaty G.; Satchi-Fainaro R.; Gozin M. *J Med Chem* **2010**, *53*, 6316.
3. Guminski Y.; Grousseau M.; Cugnasse S.; Imbert T. *Synth Comm* **2012**, *42*, 2780.

Compound 3

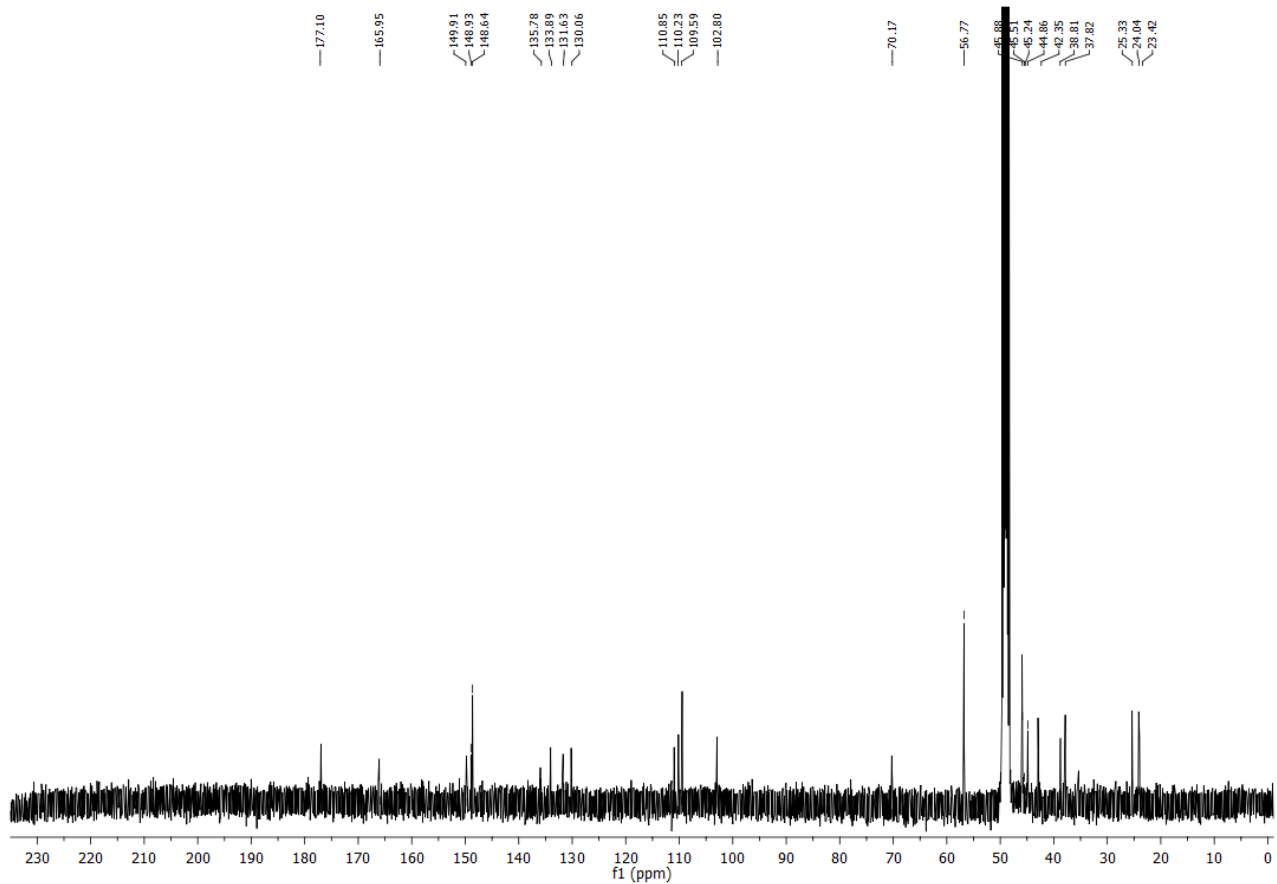
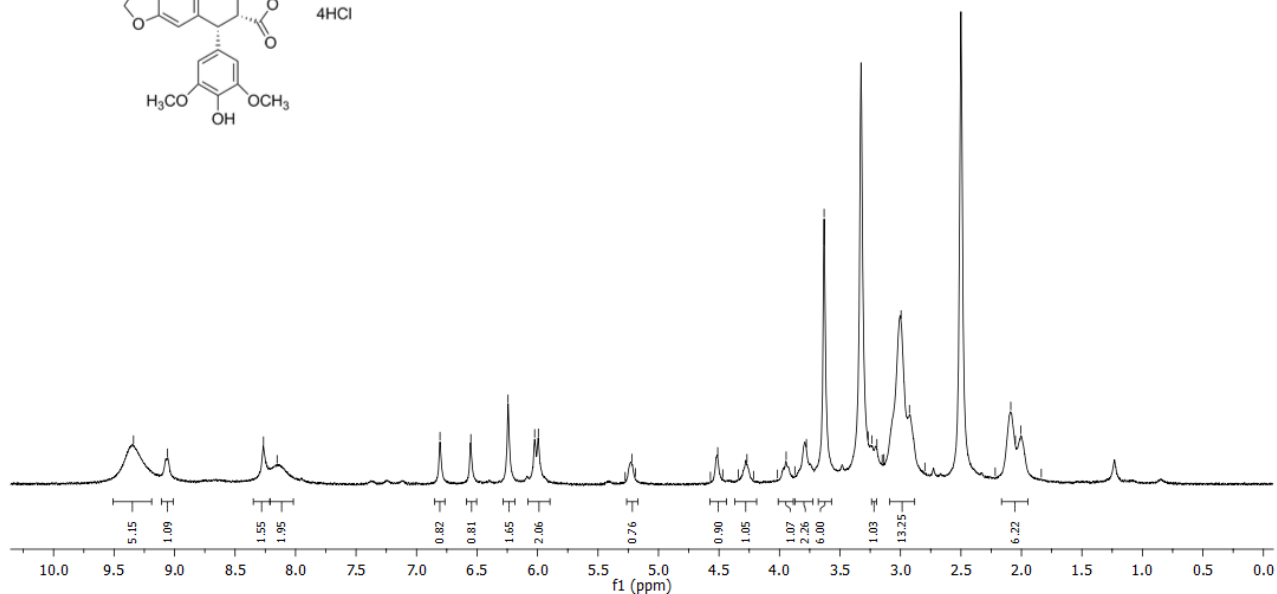
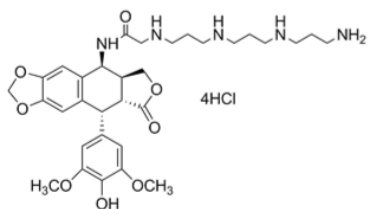


Compound 4

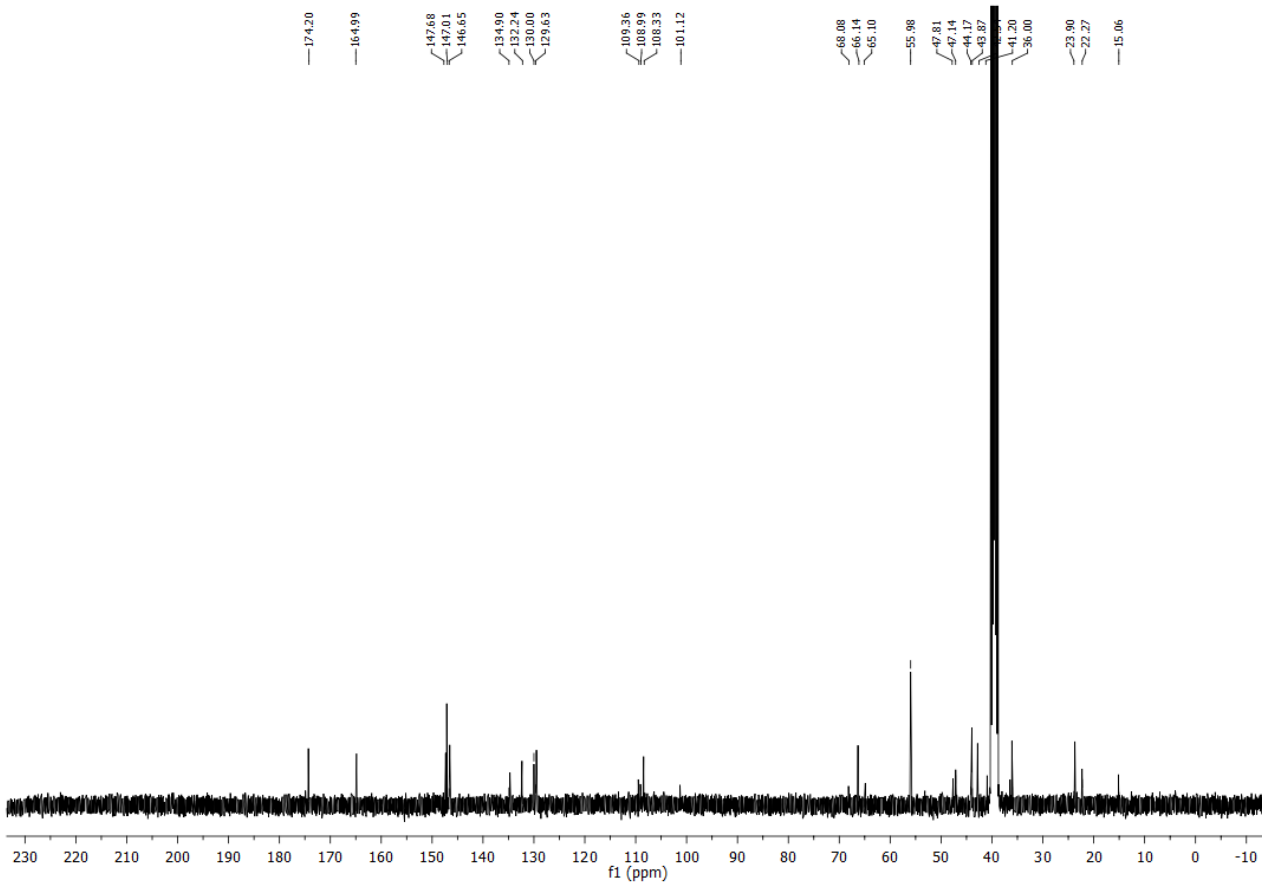
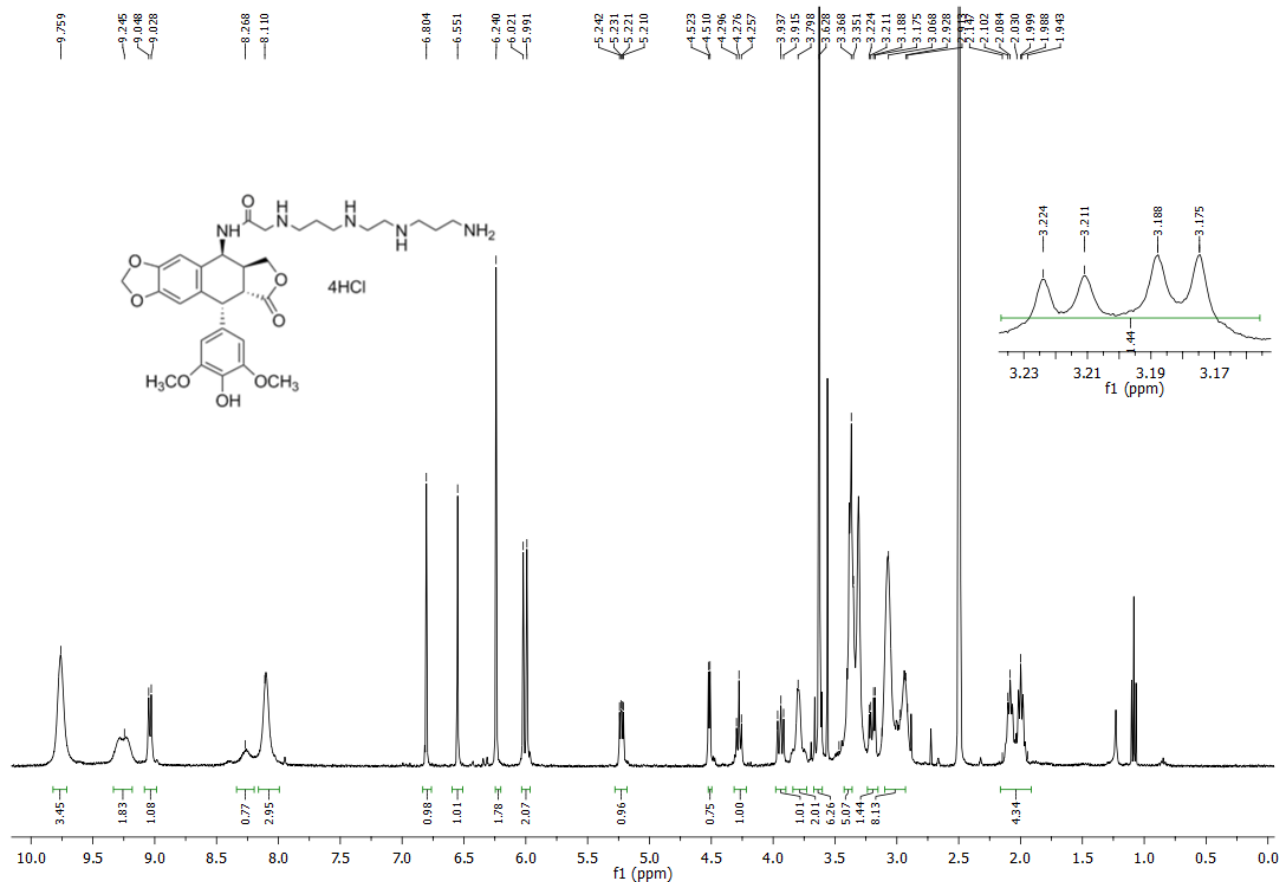


Compound 5

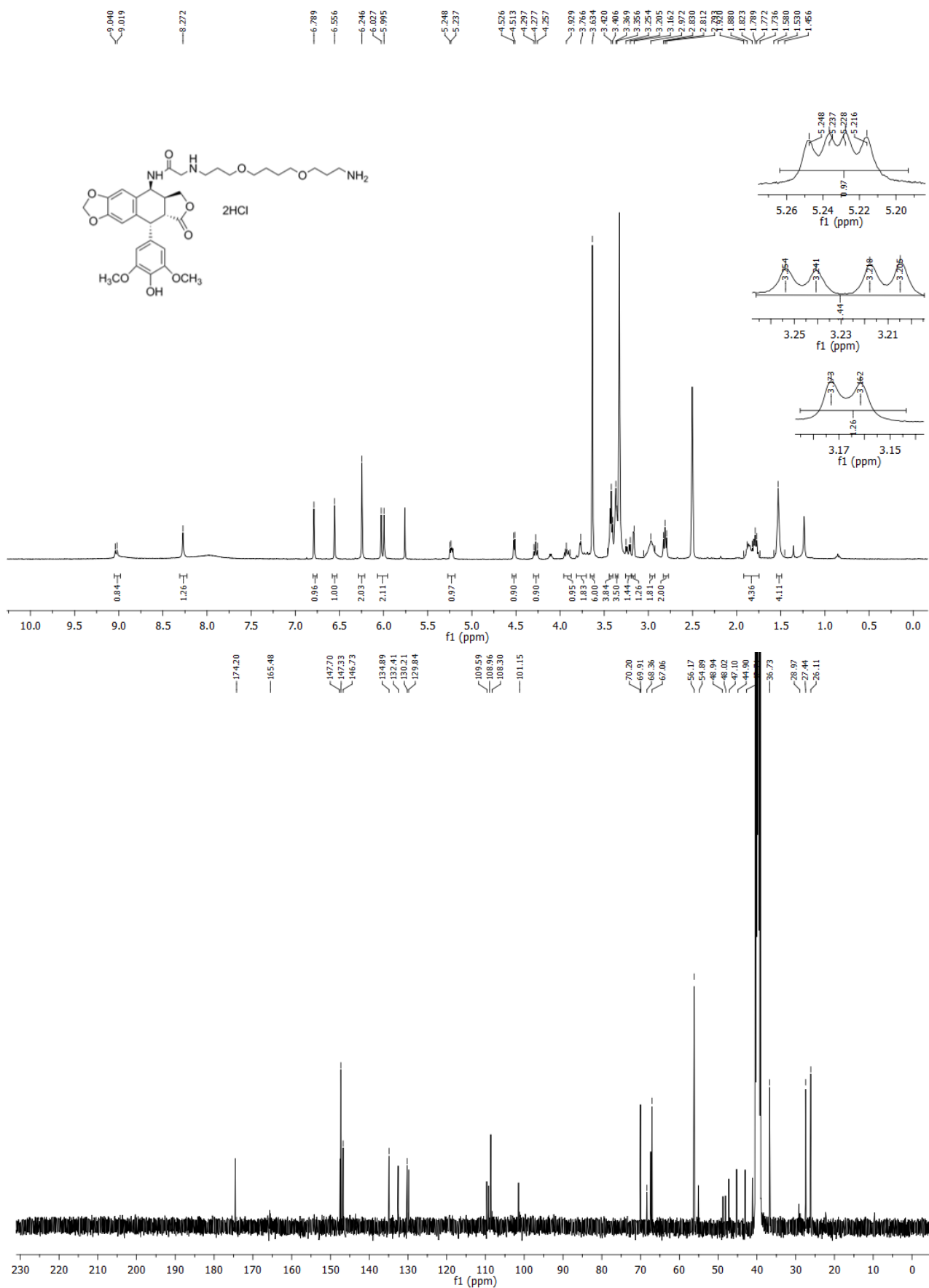
¹H NMR peaks (ppm): 9.339, 9.058, 8.265, 8.152, 6.806, 6.551, 6.244, 6.024, 5.993, 5.276, 5.218, 5.191, 4.571, 4.510, 4.469, 4.341, 4.269, 4.214, 4.016, 3.995, 3.878, 3.778, 3.631, 3.267, 3.235, 3.195, 3.151, 3.137, 2.995, 2.926, 2.798, 2.217, 2.088, 2.050, 1.895, 1.836



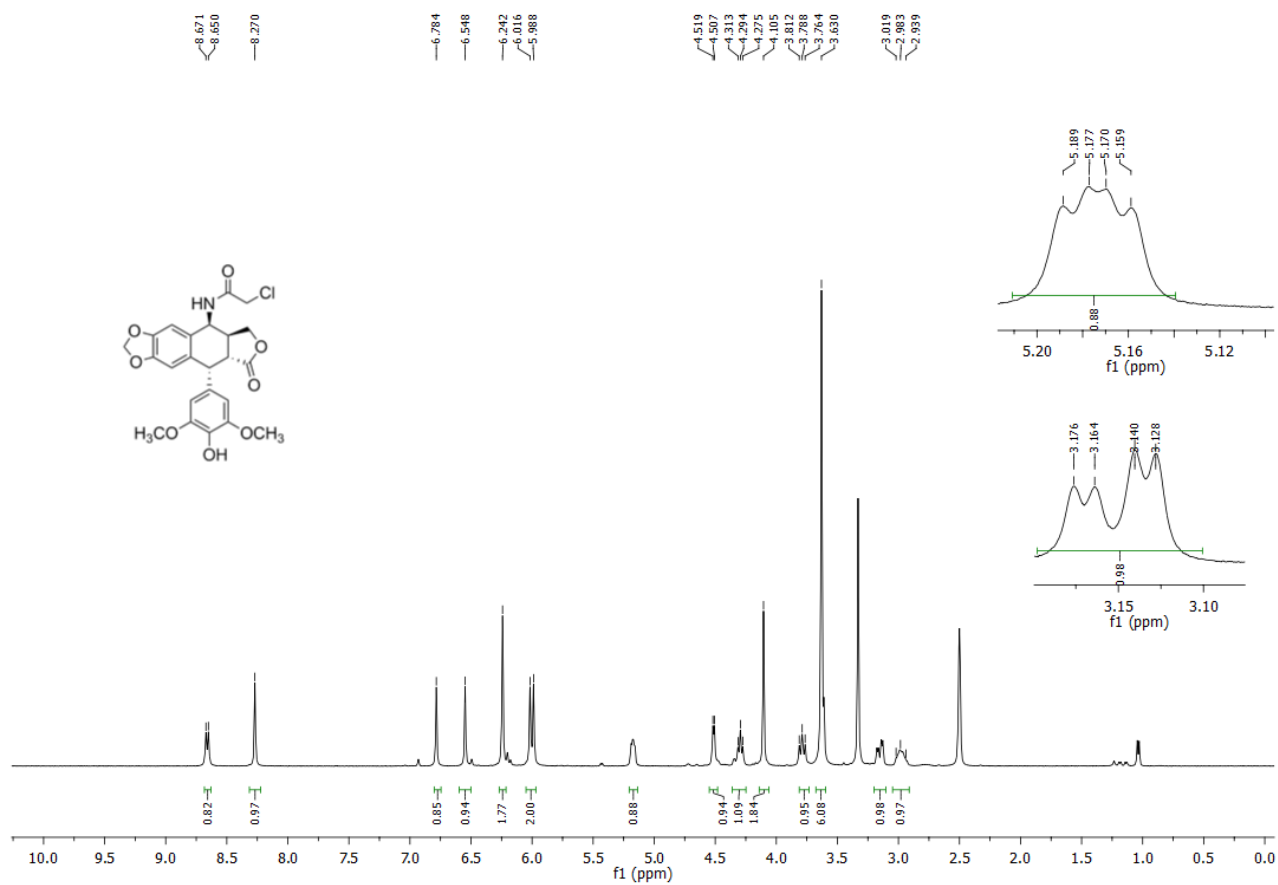
Compound 6



Compound 7



Compound 8



F14512

